

GaitGuard: Towards Private Gait in Mixed Reality

Diana Romero
dgromer1@uci.edu

University of California, Irvine

Athina Markopoulou
athina@uci.edu

University of California, Irvine

Ruchi Jagdish Patel
ruchijp@uci.edu

University of California, Irvine

Salma Elmalaki
salma.elmalaki@uci.edu

University of California, Irvine

ABSTRACT

Augmented/Mixed Reality (AR/MR) technologies offers a new era of immersive, collaborative experiences, distinctively setting them apart from conventional mobile systems. However, as we further investigate the privacy and security implications within these environments, the issue of gait privacy emerges as a critical yet underexplored concern. Given its uniqueness as a biometric identifier that can be correlated to several sensitive attributes, the protection of gait information becomes crucial in preventing potential identity tracking and unauthorized profiling within these systems. In this paper, we conduct a user study with 20 participants to assess the risk of individual identification through gait feature analysis extracted from video feeds captured by MR devices. Our results show the capability to uniquely identify individuals with an accuracy of up to 92%, underscoring an urgent need for effective gait privacy protection measures. Through rigorous evaluation, we present a comparative analysis of various mitigation techniques, addressing both aware and unaware adversaries, in terms of their utility and impact on privacy preservation. From these evaluations, we introduce **GaitGuard**, the first real-time framework designed to protect the privacy of gait features within the camera view of AR/MR devices. Our evaluations of **GaitGuard** within a MR collaborative scenario demonstrate its effectiveness in implementing mitigation that reduces the risk of identification by up to 68%, while maintaining a minimal latency of merely 118.77 ms, thus marking a critical step forward in safeguarding privacy within AR/MR ecosystems.

KEYWORDS

Gait, mixed reality, augmented reality, privacy, user identification

1 INTRODUCTION

Mixed Reality (MR) is rapidly advancing towards mainstream adoption, underscored by the introduction of devices like Apple Vision Pro [7], Meta Quest 3 [13], and Meta Aria glasses [55], succeeding the earlier released HoloLens 2 [11]. The MR market, valued at \$1.4 billion in 2023, is projected to experience substantial growth, expecting to double by 2030 [52]. MR merges the physical and digital spaces, placing virtual objects within the physical space for human interaction, facilitated by diverse sensors for hand-tracking, eye-tracking, and speech input [21]. Its applications span across various domains such as manufacturing [35, 45, 72], healthcare [40, 44, 62], and education [48, 54, 69].

However, as MR technologies integrate more into daily life, concerns about privacy and security have surfaced, especially regarding

the potential misuse of sensor data by “honest-but-curious” adversaries to extract sensitive information, including facial information [32], semantic location data [39], and user behavior [46, 49, 79]. This issue extends into multi-user MR interactions, ranging from shared physical spaces to remote collaborations, highlighting the privacy and security implications for users and bystanders alike. Recognizing these risks, research efforts have aimed to develop secure and privacy-preserving methods for MR interactions [51, 64].

Particularly concerning is the privacy of gait data within MR environments. Gait, or the manner of walking, is a recognized biometric identifier that has been used in both medical diagnosis [27] and mobile system authentication [42, 74, 75]. Gait data’s association with personal attributes such as ethnicity [78], age [80], gender [76], and health conditions [67] underscores the importance of its protection, aligned with directives like the California Privacy Rights Act (CPRA) [1] and the European Union’s General Data Protection Regulation (GDPR) [10]. Despite existing studies on securing gait data via IMU sensors [63], distance sensors [73], and mobile phones [33], the unique challenges of MR technologies demand focused attention.

This paper investigates gait privacy within the MR domain, offering the following contributions:

- (1) **Identification attack using gait features in MR:** We present the first demonstration - to the best of our knowledge - of identifying individuals through gait features *extracted from MR video feeds*, indicating potential privacy vulnerabilities.
- (2) **Assessment of different defensive mechanisms:** To mitigate identification risk, we explore various perturbation techniques for gait features, assessing their effectiveness through various privacy and utility metrics.
- (3) **GaitGuard system design and implementation:** We introduce **GaitGuard**, the first real-time solution to mitigate identification risks associated with gait features.

The rest of the paper is organized as follows: Section 2 introduces related work and background, followed by system setup and threat model in Section 3. The framework developed for extracting the gait features is explained in Section 4. Mitigation techniques with their evaluation are proposed in Sections 5 and 6. The system design and implementation of **GaitGuard** is introduced in Section 7. Finally, Sections 8 and 9 discuss the limitations, future work, and conclusion.

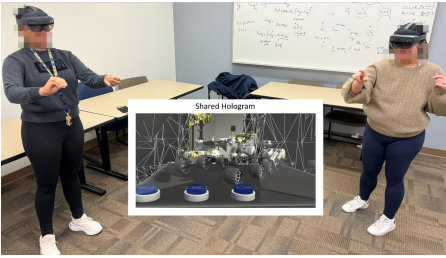


Figure 1: An example of a collaborative application in MR where two users exist in the same physical space and collaboratively work on a unified virtual object.

2 RELATED WORK & BACKGROUND

2.1 Mixed reality & collaborative applications

At the heart of immersive technologies lies Extended Reality (XR), a collective term that encapsulates the continuum of environments merging real with virtual. This continuum encompasses Virtual Reality (VR), Augmented Reality (AR), and Mixed Reality (MR), each offering distinct levels of immersion and interaction between the physical and digital worlds. Among these, MR stands out for its ability to enable direct physical interaction with virtual entities, paving the way for deeply interactive experiences.

A significant application of MR technology is in the domain of immersive **collaborative applications**. These applications exploit the spatial computing powers of MR devices, such as the HoloLens 2, to create shared holographic spaces where multiple users can interact. Through collaborative MR applications, participants can simultaneously perceive and engage with the same digital content, albeit from their own viewpoints. This capability opens new avenues for shared experiences in various fields like education, design, and remote assistance [4].

Designing collaborative experiences via MR, particularly through the Microsoft HoloLens 2, involves integrating a robust network management system. Such a system is crucial for establishing and maintaining connections among collaborating users, facilitating real-time collaboration, and ensuring consistent object behavior across the shared digital environment [4]. The HoloLens 2 leverages the Photon Unity Networking (PUN) framework to meet these needs [17]. PUN is designed to work seamlessly with the Unity development platform, a versatile cross-platform engine supporting MR/AR/VR development. The integration between Unity and PUN offers a foundation for building multi-user applications, managing network synchronization, and registering users, thereby enabling synchronized collaborative MR experiences. An illustration of a collaborative experience using MR HoloLens 2 is shown in Figure 1.

2.2 Privacy problems in mixed reality

As MR headsets become more ubiquitous, there is a growing concern about possible security and privacy risks. Among these, perceptual manipulation attacks (PMAs) represent a severe threat, altering users' perceptions and interactions within MR environments [30]. Moreover, considering these MR headsets have the unique characteristic of employing an immersive multi-user collaborative interaction, there is a growing concern about ensuring

secure and private interactions in collaborative environments. In response to this concern, SecSpace, a framework developed to ensure privacy and security mechanisms are implemented in collaborative MR, has been proposed [64]. Beyond the individual user, the issue of bystander privacy emerges as a critical concern, underlined by the inherent functionalities of MR headsets. These devices, equipped with sensors, inadvertently intrude on the privacy of non-consenting individuals in their vicinity by collecting images, videos, and audio data [32]. Although the issue of bystander privacy has been extensively examined for decades in the context of mobile devices, it has recently gained prominence in augmented reality headsets, with studies like BystandAR exploring solutions specifically for facial privacy [32].

The literature identifies three targets of privacy vulnerabilities within MR: (1) the headset wearers, (2) other MR participants in a collaborative environment, and (3) bystanders. While existing research examines privacy threats and mitigation strategies across the three targets, the protection of **gait privacy** within the MR technology remains markedly under-explored. **This paper seeks to fill that gap in the existing body of research, particularly the gait privacy of MR participants and bystanders.**

2.3 Gait: a unique personal signature

Gait recognized as an inherently unique attribute for individuals has been extensively studied as a means of authentication, both through wearable devices, such as accelerometer sensors [31, 36, 43] and mobile systems, such as phones and smartwatches [25, 34, 56]. These studies underscore gait's potential for reliable identification, spotlighting the privacy concerns that arise from its use.

The analytical potential of gait extends well beyond primary identification purposes. It has been empirically shown to correlate with sensitive personal attributes, including ethnicity [78], age [80], gender [76], and neuromusculoskeletal disorders [67]. In light of these considerations, regulatory measures such as the California Privacy Rights Act (CPRA) [1] and the European Union General Data Protection Regulation (GDPR) [10] have ensured the protection of biometric data, including gait. These legal frameworks emphasize the demand for privacy-preserving practices in collecting, storing, and utilizing gait data across technological applications.

Prior research has proposed various methodologies for securing gait data, including the utilization of worn IMU sensors [63], distance sensors [73], and mobile phones-based approaches [33]. Despite these advancements, the exploration of gait within MR environments remains underrepresented in the current literature. **To the best of our knowledge, no study currently systematically investigates and mitigates the prevalence of identification attacks using gait in the realm of MR.**

2.4 Pose estimation for gait detection

Instrumented gait analysis (IGA) is the precise and accurate analysis of gait patterns and characteristics. IGA systems often employ motion capture systems, force plates, instrumented walkways, and treadmills [29]. While this is the golden standard for gait assessment in research practice, these IGA systems are costly and invasive. Accordingly, alternative techniques for cost-effective gait analysis

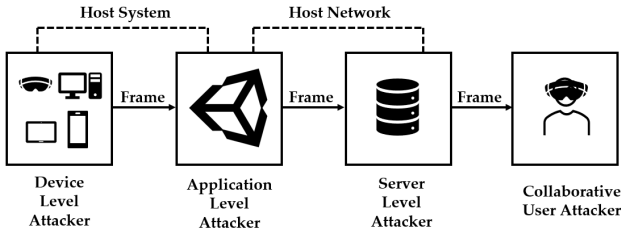


Figure 2: Flow of camera frames in MR and possible vantage points.

have been proposed, such as using gyroscope [59], inertial measurement units (IMU) [61], and Kinect sensor [41, 60]. Another low-cost and accurate alternative is video-based pose estimation [53, 68]. Video-based methods are particularly accessible, requiring only camera feeds to analyze gait. Through pose estimation algorithms, this technique interprets a subject’s position and orientation by predicting the locations of body keypoints, including the hands, head, and legs [18]. Openpose, a state-of-the-art tool in the field of pose estimation, enables pose estimation of multiple people from a two-dimensional video [28]. This has been evidenced by the work of Stenum et al., who showcased that video-based gait analysis via Openpose can approximate the accuracy of more traditional 3D motion capture analyses [68]. This paper leverages video-based gait analysis using Openpose for its accessibility and effectiveness [68].

3 THREAT MODEL & MR SYSTEM SETUP

This paper investigates the threat of identification attacks through gait features in MR applications, mainly through video-based gait feature extraction. The focus is on head-mounted devices (HMD), such as the HoloLens, which are equipped with two types of cameras, facilitating communication with other devices such as MR headsets, phones, tablets, and laptops¹. The dissemination of camera frame feeds in MR ecosystems constitutes a potential vantage point for adversaries to capture and analyze gait features.

Targeted victims. As motivated in Section 2.2, since the camera of the current MR devices, such as HoloLens 2, are world-facing, the target victims of the threat of identification through gait feature extraction are other MR participants engaged in a collaborative MR environment, along with bystanders that are in the view of the outward-facing camera.

Significance. The access to camera frames, while crucial to ensure correct functionality in these MR applications, also threatens the participants’ privacy. A survey of 318 HoloLens applications from the Microsoft Store [14] showed that 26% request camera access, underscoring the widespread exposure of users to the threat of gait feature extraction.

3.1 Threat model

The multifaceted threat model proposed is visually shown in Figure 2, encapsulating the following dimensions of vantage points:

¹While the rest of the paper focuses on HoloLens as an example of HMD, the same analysis/results can be extended to other HMD in the market that need to share scene information across users collaborating in a multi-user MR environment.

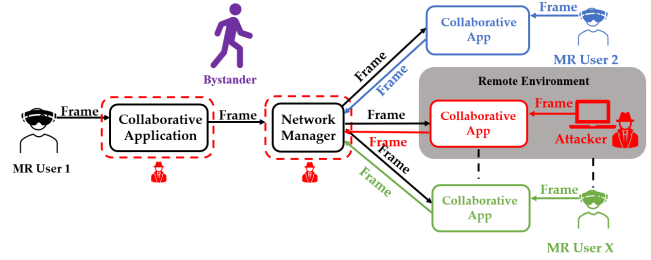


Figure 3: Threat model in different MR application setups. Possible targets are other MR participants in a collaborative MR environment and bystanders.

- **Device level:** An adversary possesses either access to or control over the MR device’s firmware, enabling direct extraction of raw camera frames.
- **Application level:** Adversaries exploit vulnerabilities within the application to access camera frames. These applications require access to camera frame feeds for functionality.
- **Server level:** In scenarios where camera frames are shared across a network, adversaries with access to the server or an “honest-but-curious” server can execute the attack. Adversaries can intercept and access the shared camera frames by installing spyware or exploiting vulnerabilities on the server, compromising the privacy of all participants in the collaborative space.
- **Collaborative user attacks:** Given the architecture of MR applications, which stream camera frames to all collaborating devices, any participant — connecting via MR headsets, smartphones, laptops, or tablets — might not just be a benign collaborator but could also exploit the shared visual data to perform gait identification attacks on other users.

3.2 MR system setup & potential threat scenarios

Based on the discussed threat model and our targeted victims, we define three primary MR application setups explored as potential threat scenarios summarized in Figure 3:

- **Single user experience (SUE):** This application setup is not designed for collaboration. The application needs access to the camera to enable virtual overlays. This introduces a critical concern regarding **bystander privacy**, where individuals unintentionally share the same physical space as the MR application user. The adversary in these applications can exist on the device and application level (shown in Figure 2), with the target being the bystanders.
- **Same physical space collaboration (PSC):** This collaboration mode enables users within the same physical space to interact with shared virtual content. Applications exemplifying this setup may also integrate augmented reality features necessitating camera access, such as HoloOne Sphere [20] and Catapult [9]. The shared camera feeds across multiple devices to the common network manager server, as explained in Section 2.1, heightens the vulnerability to device, application, and server-level attacks targeting bystanders and other MR participants.

- **Remote space collaboration (RSC):** Distinguished from **PSC** by the allowance for remote user participation, this setup exposes additional vulnerabilities. Any device, not limited to MR headsets, participating in the session can access the camera feeds of all users, introducing a new axis of potential adversarial action across device, application, and server levels and from collaborative external users. Examples of this application setup that enable remote collaboration are Lens Bouvet [8] and Teams [16], which request camera frames to allow **RSC** and annotation of an MR headset’s view.

3.3 Adversary model

We assume the adversary can run any classification model for identification using gait features extracted from camera frames acquired through any of the vantage points described in Section 3.1 and within any of the potential threat scenarios described in Section 3.2. More details on the adversary model will be discussed in Section 4.3 and Section 5.3.

4 GAIT EXTRACTION FRAMEWORK

In this section, we discuss the systematic design and implementation of the framework used to gather the targeted victim’s gait features, which we refer to as **GaitExtract**. As mentioned earlier in Section 2.4, our design adapts and modifies the method developed by Stenum et al. where they proposed to use 2D-based techniques for gait feature analysis [68]. Their proposed algorithm generates the different gait features based on the location of specific keypoints provided by OpenPose library [68].

4.1 User study and data collection

We conducted an IRB-approved user study (IRB #2848) where 20 participants were recruited by advertising on mailing lists and asking personal contacts to forward our study information to interested participants. Eligibility was confined to those aged 18 and above. Before data collection, participants were briefed about the study’s objective of exploring the implications of gait feature privacy within the MR environment. It was emphasized that all personal identification information would be stripped from the collected data, ensuring that only the research team could access it. Participants gave their written consent granting permission to videotape their gait sequences. Participants were given face masks as an extra precaution to prevent recording their facial information during the data collection. Participants were also invited to complete a brief survey to capture their perceptions and concerns regarding gait privacy in MR settings.

Data collection consisted of participants walking for about 5 minutes between two markers in a private room while a research team member wore the HoloLens 2 to record their walking sequences. Figure 4 illustrates the data collection setup. Because of the two markers’ position, the distance of the user’s walking sequences was between 2.5m and 2.75m. This limited distance was chosen deliberately, aligning with the expectation that users engaging in MR collaborative activities would not necessitate extensive movement. Furthermore, this setup aimed to investigate the potential of distinguishing an MR user based on gait features, even over relatively short distances.

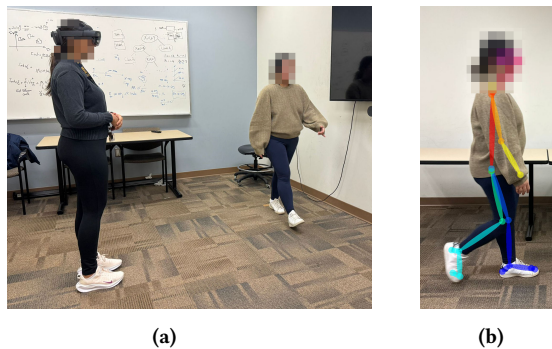


Figure 4: Data Collection Setup; (a) Recording of walking sequence; (b) Application of OpenPose to a walking sequence.

The number of participants is on par with related work that focused on protecting bystander visual data in augmented reality, which consisted of 16 participant [32]. It is important to note that developing a gait feature dataset is not the focus of this paper. Instead, it serves primarily to assess the practicality of identifying individuals through their gait features.

4.2 Gait feature extraction

4.2.1 Video-based analysis of human gait using pose estimation.

This paper adapts the video-based gait analysis tool developed by Stenum, et. al., which has demonstrated comparable performance with state-of-the-art gait analysis methods in the medical community [68]. The tool uses the *keypoints* identified by the OpenPose library as a basis for the gait feature extractions. Specifically, it utilizes 3 out of the 25 body keypoints identified by OpenPose, the midhip, left ankle, and right ankle, for its analysis.

This tool was designed to be applied to a single video of a walking sequence, where a walking sequence refers to an instance or video of a person that walks exclusively in one direction. Several manual interventions are required for the gait feature extraction. Firstly, the tool needs manual labeling of the walking direction of the subject (i.e., left to right or right to left). Next, any inaccuracies in detecting the left and right legs need manual correction. Thirdly, manual pinpointing of the heel-strike and toe-off of each leg is essential. This is crucial as heel-strike and toe-off are two events that make up a gait cycle [58]. After correcting the leg identification, the positions of two distinct markers must be chosen manually from the video frame, and the distance between them must be entered. This step is critical for the tool to estimate the distance per pixel, which aids in calculating the step length.

Upon completing these manual procedures, the tool is capable of producing a set of gait features for each leg and for every walking sequence, noting that a walking sequence comprises several gait cycles. A full gait cycle is defined to be when the same leg can complete at least two consecutive toe-offs or heel-strikes [71]. For each sequence, the tool outputs an array of vectors, with each vector encapsulating 10 distinct gait features. These features are visually illustrated in the Appendix A.

- **Left and Right Step time:** Time in seconds between consecutive bilateral heel-strikes.

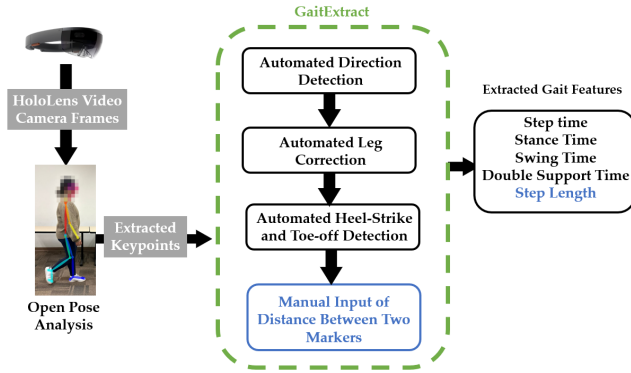


Figure 5: GaitExtract: A gait extraction framework built on the OpenPose library. GaitExtract uses camera frames obtained from the HoloLens. The automated feature extraction algorithm uses the keypoints generated by OpenPose to extract the gait features. The manual input of distance between two markers is only necessary when the step length feature is desired.

- Left and Right Stance time: Time in seconds between heel-strike and toe-off of the same leg.
- Left and Right Swing time: Time in seconds between toe-off and heel-strike of the same leg.
- Right to Left and Left to Right Double support time: Time in seconds between heel strike of one leg and toe-off of the contralateral leg.
- Left and Right Step length: Distance in meters between the ankles at heel-strike.

4.2.2 GaitExtract: Adapted gait feature extraction. To exploit this tool for gait feature extraction in MR applications, it must be automated and adapted to the MR setup. Accordingly, we propose **GaitExtract** framework as shown in Figure 5. **GaitExtract** takes a walking sequence video captured using the HoloLens headset as an input and then applies the OpenPose algorithm to generate the pose keypoints. These keypoints will then be used to calculate the different gait features. Notable adjustments are made to automate the tool, such as (1) automation of walking direction identification (left to right or right to left), (2) automation of the correction of the left-right leg identification, (3) automation of the detection of the heel-strike and toe-off events, (4) automation of running the gait feature extraction for multiple walking sequence, and (5) automation of detecting insufficient data to represent a complete gait cycle in a walking sequence.

GaitExtract framework is designed to operate in two modes: fully automated and partially automated. In its fully automated form, **GaitExtract** computes all gait features except for step length without manual intervention. Conversely, the partially automated mode can generate all gait features but necessitates minimal user contribution. Specifically, manual intervention is needed to analyze the initial walking sequence for each participant to identify marker positions and the distance essential for step length computation. This manual step is crucial for accurately calculating the step length feature, hence the requirement for limited manual input

in this mode. Subsequent sections, particularly Section 4.3, will evaluate the role and impact of the step length feature in individual identification.

4.3 Identification via gait features

4.3.1 Identification model implementation. We use the gait features produced by **GaitExtract** using data from the 20 participants in our user study. As mentioned in Section 3.3, an adversary can run any classification model for identification. To showcase this, we used GradientBoostingClassifier provided by the scikit-learn library in Python because it showed the best identification accuracy among the readily available models in Python’s scikit library [19]. As mentioned in Section 4.2, we can have a fully- or partially-automated **GaitExtract** framework. Hence, we trained the classifier using data with and without step length to compare the performance of **GaitExtract** in identifying people.

4.3.2 Uniqueness of gait features across individuals. Results show that the classification model trained without step length gives 68% accuracy and that the classification model trained with step length gives 78% accuracy in user identification. In particular, it was observed that User 5 had the lowest classification accuracy of 52.59%, which can be attributed to the fact that User 5 had the least amount of gait features. Since all the 20 participants walk the same distance $\approx 2.5m - 2.75m$ back and forth within fixed time $\approx 5min$ as mentioned in Section 4.1, the total number of generated gait feature vectors among the participants highly varied², where the least number of gait vectors produced by one participant was 78. The maximum number produced was 204. This high variation in the total count of gait vectors produced is caused by the different ways people walk. A person with a small step length and walking fast would have many more extracted features than a person with a longer step length and walks slowly in the same duration.

This high variation of gait feature vectors can be addressed with data augmentation methods, such as random oversampling. Results show that the classification model trained on augmented data without step length gives 88% accuracy and that the classification model trained on augmented data with step length gives 92%. Figure 6 shows the average confusion matrix of the classifier on augmented data **without step length**. More details on the training of the classification model and the accuracy of the different classifiers in identifying participants using gait features are in Appendix B.

An analysis of the top 3 unique gait features for each participant can be seen in Figure 7. Results show that the top 3 unique gait features are not consistent among individuals, highlighting the finding that the gait features extracted using **GaitExtract** are identifying.

These results show that an off-the-shelf classifier, specifically GradientBoostingClassifier, can uniquely identify people with reasonable accuracy when using a partially automated **GaitExtract** (with step length) as well as using a fully automated **GaitExtract** (without step length). Results also show that the number of gait features per individual heavily influences inter-class classification accuracy.

²Each gait feature vector encapsulates 10 gait features for each walking sequence as described in Section 4.2

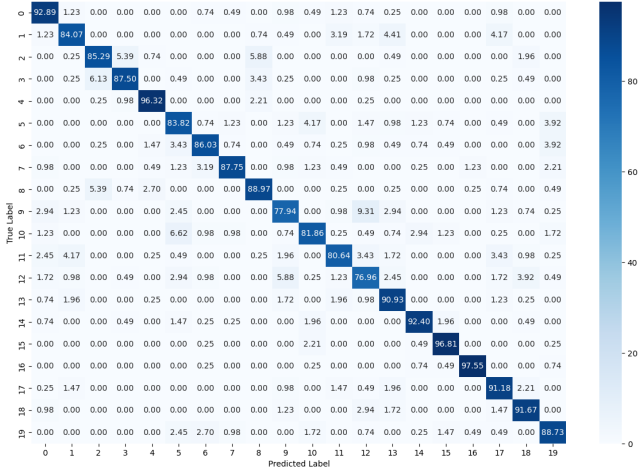


Figure 6: Average confusion matrix across all folds on data without step length.

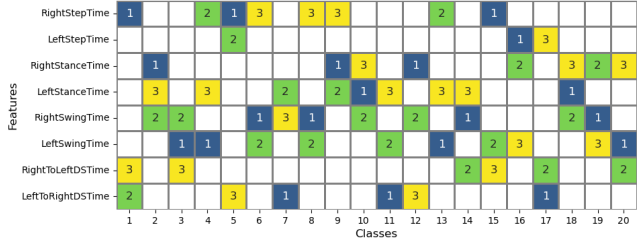


Figure 7: Top 3 unique gait feature for each participant.

To the best of our knowledge, these results show for the first time the feasibility of identification of individuals using video-based gait feature extraction in MR applications.

5 MITIGATION FRAMEWORK

This section presents, evaluates, and compares a range of mitigation techniques for target identification through gait features operating on the video frame. In particular, we explore two axes for mitigation: first, investigating where to apply the mitigation in the video frame, and second, exploring what type of mitigation can be applied.

5.1 Location: Where to apply the mitigation?

We propose two approaches for mitigation at different location granularity in the video frame based on **GaitExtract**, namely **keypoint-based masking (KPM)** and **lower body-based masking (LPM)**.

(1) **Keypoints-based masking (KPM)**: Since **GaitExtract** utilizes data from three keypoints, we conducted experiments involving applying mitigation methods on different combinations of keypoints.

- **KPM**: This defense involves applying mitigation on the area surrounding the three keypoints involved in gait feature extraction (midhip, left ankle, and right ankle). This is driven by the hypothesis that obfuscating the detected keypoints for gait feature extraction can confuse the adversary.

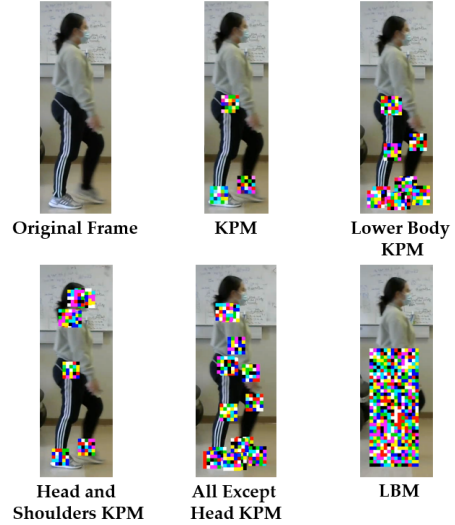


Figure 8: Example video frame for each of the mitigation locations.

- **Head and shoulders KPM**: This uses the key points in KPM and the head and shoulders key points. The goal is to investigate if the obfuscation of parts of the upper body affects user identification through gait features.
- **Lower body KPM**: This defense uses the keypoints in KPM plus the hips, knees, heels, and toes. Since walking is mainly a lower body activity, we investigate the efficacy of applying mitigation on all the lower body keypoints.
- **All except head KPM**: This variation obscured all the keypoints except the head.

To identify how much of these keypoint areas need to be obfuscated to confuse the adversary effectively, the mitigation area surrounding the keypoints varied. In particular, for **KPM**, a `box_length = 50, 100, 150, 200` pixels were explored, and for **Lower body KPM**, **Head and Shoulders KPM**, and **All except head KPM**, a `box_length = 50, 100, 150` pixels were explored. **KPM** uses a larger set of `box_length` because it only uses three keypoints that are far apart, minimizing any overlap in the area mitigated.

- (2) **Lower body-based masking (LBM)**: Since **GaitExtract** derives information solely from the lower half of the body, we conducted experiments involving applying mitigation methods on a bounding box surrounding the lower half of the body. This approach is closely related to the **Lower body KPM** method with a large enough box size surrounding the keypoints, but this approach removes the necessity of using **OpenPose** to identify keypoints as part of **GaitExtract**.

These two approaches, highlighting the location of where to apply the mitigation, are shown in Figure 8, providing a visual representation of the mitigation in a video frame.

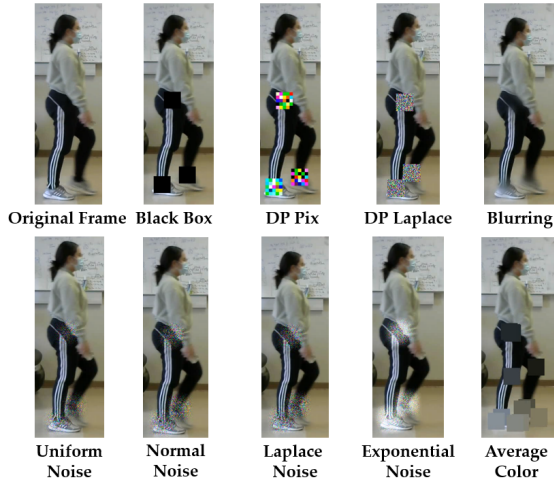


Figure 9: Example video frame with the mitigation types we apply.

5.2 Type: What mitigation to apply?

Numerous strategies exist within the domain of mitigation for safeguarding camera frames or photos, such as adversarial mitigation [77], privacy-preserving GANs (Generative Adversarial Networks) [66], human-imperceptible privacy protection [65] and quantization [50]. A drawback of many of these strategies is that they are resource-intensive and not optimized for real-time applications. In this paper, we deliberately investigate fundamental mitigation methods and the effects of these methods in fortifying privacy in conjunction with utility and their potential for real-time applications. Particularly, we explored the following mitigation types with examples in Figure 9.

- (1) **Black box:** This defense is adapted from the work proposed by Corbett et al. in BystandAR [32] where a black box was applied on sensitive regions to protect facial privacy. The pixels of the KPM and LBM regions of interest are changed to black. This is also used as a *baseline* to compare the performance of the other mitigation techniques.
- (2) **Differentially private pixelization (DP Pix):** This defense is adapted from the work proposed by Fan et al., where it guarantees that two “neighboring images” with the same dimension differing by at most m pixels are indistinguishable [38]. While their results focused on grayscale images, they noted that the algorithm can be applied to RGB images by applying it to each channel separately. Thus, in this mitigation approach, *DP Pix* was adapted as follows: (1) Identification of m representing the number of pixels in the area of interest identified by KPM or LBM. (2) Pixelization of kernel size b within the area m . (3) Application of the Laplace mechanism to each pixelized cell of size $b \times b$ with the scale parameter equivalent to $\lambda = \frac{3 \times 255 m}{b^2 \epsilon}$ for each red, green, and blue channel. In the case of KPM, $m = \text{keypoint_count} * \text{box_length}^2$ where *keypoint_count* refers to the number of keypoints used out of the 25 Openpose keypoints used for the mitigation and *box_length* refers to the length of the square area surrounding

the key points. Similarly, in LBM, m is equivalent to the area of the lower body. In our experiments, we choose $\epsilon = 0.1$ and explored kernel sizes $b = \{10, 20, 30, 40, 50\}$.

- (3) **Differentially private Laplacian noise (DP Laplace):** This defense is grounded from work proposed by Fan et al. [38] using their notion of m -neighborhood images where instead of applying the DP mechanism on each pixelized cell, it is applied to each pixel of interest. This defense involves the following steps: (1) Identification of m number of pixels of interest in each k keypoint region of interest. (2) Calculation of global sensitivity Δf based on k and m . (3) Application of the Laplace mechanism to each pixel m in each k keypoint regions of interest with the scale equivalent to $\lambda = \frac{\Delta f}{\epsilon}$ for each red, green, and blue channel. In our experiments, we explored $\epsilon = 0.1, 10, 100, 1000$. In the case of LBM, $k = 1$, and m is the number of pixels in the lower body.
- (4) **Gaussian blur:** Blurring is another common image mitigation technique we adopted. This is a common way to remove sensitive information from video content and is predominantly used in YouTube’s face-blurring feature for content creators [22]. To investigate the capability of this defense in protecting gait privacy, we adapted Gaussian blurring as follows: A 2D Gaussian kernel of size $c \times c$ and standard deviation of 0 is used for blurring. We explored $c = \{5, 25, 45, 65\}$ in our experiments.
- (5) **Random noise:** Four types of random noise characterized by varying the distribution parameter denoted as λ were used to introduce noise to each pixel of the KPM and LBM regions. The random noises were applied with a hanning window to smooth the edges. We explored four different values for $\lambda = \{50, 100, 150, 200\}$ for the following random noise distributions: Uniform noise distribution with a range $[-\lambda, \lambda]$, normal noise distribution with a standard deviation of λ , Laplace noise distribution with a scale parameter λ , and exponential noise distribution with a rate parameter λ . More details on the probability density distribution of these noises are in Appendix C.
- (6) **Average color:** This defense involves applying the average RGB color of the pixels in the region of interest. The idea is that it obfuscates the area of interest without drastically changing the color.

Hence, across various locations (Section 5.1) and types of mitigation with different parameters (Section 5.2), we will evaluate a total number of 248 combinations of mitigation techniques.

5.3 Evaluation Strategy & Metrics for Mitigation Techniques

In this section, we outline the strategy we use to evaluate the various mitigation techniques, and in Section 6, we will discuss in detail the numerical results of the evaluation.

5.3.1 Adversary model. In the domain of biometric data privacy, there exists a significant body of research focusing on the anonymization of such data, with many studies employing recognition or identification models trained on unaltered/clean data to evaluate the effectiveness of anonymization techniques [26, 70]. Nevertheless, more recent studies have shown that models trained on data already subject to anonymization or mitigation efforts offer more robust

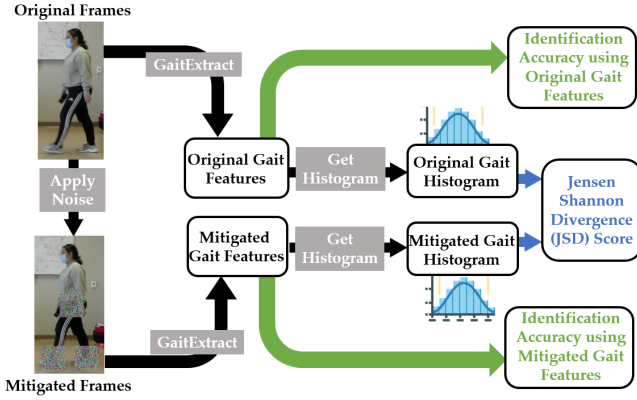


Figure 10: An illustration of the mitigation and evaluation framework. Mitigation is first applied to the original camera frames to generate the mitigated frames. GaitExtract is applied to the original and mitigated frames to generate gait values. Identification is then done on the original and mitigated gait values. The JSD Score is calculated for the original and mitigated gait values.

performance. To evaluate the implications of these two approaches, this paper outlines two distinct adversary models reflective of differing levels of access and awareness regarding the deployment of mitigation techniques:

- **Weak adversary.** We consider an adversary that initially has access to clean camera frames from the MR headset and becomes unaware that mitigation or anonymization techniques are “later” on applied. Thus, the adversary can train an identification model using the clean gait features.
- **Strong adversary.** We focus on evaluating the different mitigation techniques against a strong adversary who is aware that the camera frames are mitigated and, therefore, trains an identification model on perturbed gait features.

The discussion in this paper focuses on the strong adversary as it has shown that recognition models trained on mitigated data are more resilient against mitigation [47]. However, a comparison between the evaluation results of two types of adversaries will be highlighted in Section 6.1.

A pictorial overview of the mitigation process and its evaluation in the context of a strong adversary is shown in Figure 10. The mitigation process involves the application of noise to the original frames (as explained in Section 5), followed by utilizing the **GaitExtract** framework on both the original and mitigated frames. The gait features obtained from the original frames are denoted as G , encompassing an array of gait vectors where each vector contains various gait features, including step time, stance time, swing time, double support time, and step length for both the left and right leg, as mentioned in Section 4.2. Similarly, the gait features derived from the mitigated frames are denoted as G' . We used quantitative and qualitative metrics to assess the efficacy of the applied mitigation in safeguarding gait privacy.

5.3.2 Privacy loss metrics. We use two metrics to quantify the privacy loss as follows:

- **Jensen-Shannon divergence (JSD) score:** The JSD score is computed based on the histograms of gait features in G and G' . The JSD score offers insights into the similarity or dissimilarity of the distributions of gait features. A JSD score of 0 indicates an identical histogram distribution, signifying perfect similarity, while a score of 1 suggests a completely different distribution, indicating maximum dissimilarity. This metric evaluates how the gait features are perturbed considering that an adversary whose purpose is not just to do identification but other gait feature analysis, as motivated in Section 2.3.
- **User identification accuracy:** User identification is performed using the gait features (G) and (G') employing the identification technique outlined in Section 4.3. In particular, we want to evaluate how the mitigation techniques impact the accurate identification of individuals based on their gait features by getting the difference in identification accuracy using clean (G) and mitigated (G') data. The reduction in user identification results provides insights into the practical implications of the mitigation strategies on the overall effectiveness of gait-based identification systems.

5.3.3 Utility metrics: We use several metrics for the utility to assess the privacy-vs-utility tradeoff (PUT) as follows:

- **Peak signal-to-noise (PSNR):** To quantify the utility of the mitigation, we measured the change in the quality of the video post-mitigation by measuring the peak signal-to-noise (PSNR) of the modified pixels along the red, green, and blue channel of each frame.
- **Structure similarity index (SSIM):** We also evaluated the difference in the luminance, contrast, and structural information between the original G and the mitigated frame G' by measuring the SSIM [24].
- **System metrics:** Furthermore, to quantify the utility of the system implementation, we measured the application frame rate (fps) and the latency at each point of receiving the camera frame. We evaluated the frame rate and the latency in Section 7.
- **Qualitative measures:** We used qualitative metrics to assess our mitigation strategy by conducting a user survey on the 20 participants. The results of this survey will be discussed in Section 7.1.4.

6 EVALUATION

We report the evaluation results of different mitigation techniques against the metrics discussed in Section 5.3. First, we discuss the performance of the mitigation techniques against the two types of adversaries, and then we observe the effect of the different approaches in the distribution of the gait features. Lastly, we evaluate the privacy-utility tradeoff of each technique.

6.1 Weak vs. strong adversary

The weak versus strong adversary results show consistent observation with the work done in [47]. In summary, the results show that on average (across all 248 mitigation techniques mentioned in Section 5), the weak adversary’s identification accuracy was 20% less than the strong adversary. This underscores that if an adversary knows that mitigation is applied and trains the identification model on mitigated data, it will be resilient and still do the identification

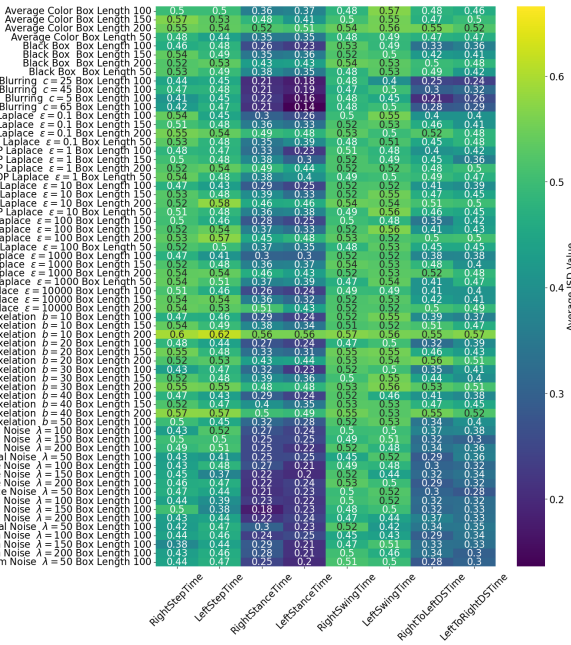


Figure 11: JSD heatmap of KPM mitigation.

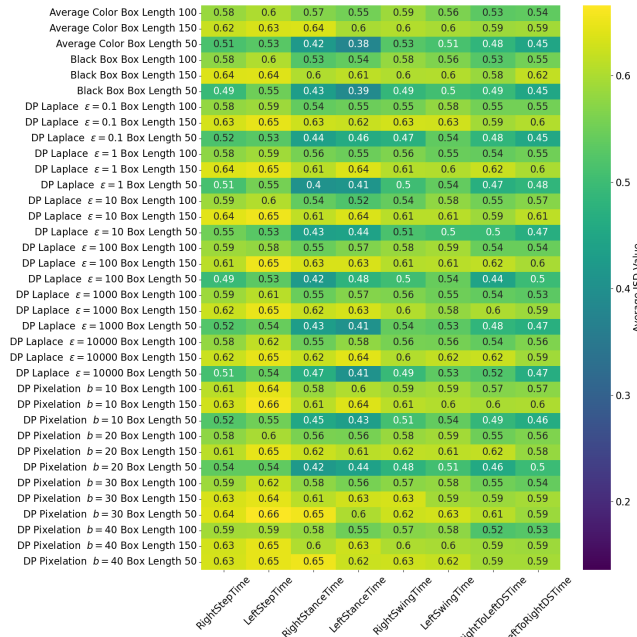


Figure 12: JSD heatmap of KPM lower body mitigation.

task. Thus, to investigate the robustness of the different mitigation techniques, the rest of the paper will focus on the results of the strong adversary. More details on the weak adversary results are in Appendix D.

6.2 Mitigation techniques effect on gait features distribution

To observe each mitigation technique’s effectiveness in changing the gait feature distribution, we used the first privacy loss metric (explained in Section 5.3.2) measured through the JSD across all features and all 20 participants. Figure 11 shows the heatmap of the JSD values for the KPM mitigation. The low JSD values of KPM indicate that KPM has the least effect on shifting the distribution of the gait features, with most JSD values being less than 0.5. This can be attributed to the fact that OpenPose can interpolate the locations of the three keypoints that are mitigated (midhip, left, and right ankle) based on the location of the other keypoints (i.e., knee, torso, head). In particular, the JSD values for the blurring and random noise mitigation types had the lowest JSD values, suggesting that these mitigation types are ineffective for keypoint-based mitigation. Hence, we focus on other mitigation types for the rest of the KPM locations.

Conversely, adding more keypoints to mitigate increases the JSD score as in “lower body KPM” and “all except head KPM”. However, the extent of keypoint masking does not proportionally affect the distribution of gait feature data. In particular, the JSD scores for the “lower body KPM”, depicted in Figure 12, range from 0.47 to 0.63. These scores are close to those recorded for the “all except head KPM”, which vary between 0.46 and 0.64.

On the other hand, applying mitigation using “lower body-based masking (LBM)” that does not depend on keypoints shows a JSD score of values ranging from 0.34 to 0.63, which shows that the JSD result depends on the type of mitigation. A more detailed examination of the JSD scores with their heatmaps associated with other mitigation locations and types is available in Appendix E.

Among all the combinations of mitigation, we observed that the mitigation technique average color applied at LBM and *DP Pix* applied at LBM are two of the techniques that show the highest shift in the gait feature distributions as indicated in the highest JSD score.

6.3 Privacy-utility tradeoff (PUT)

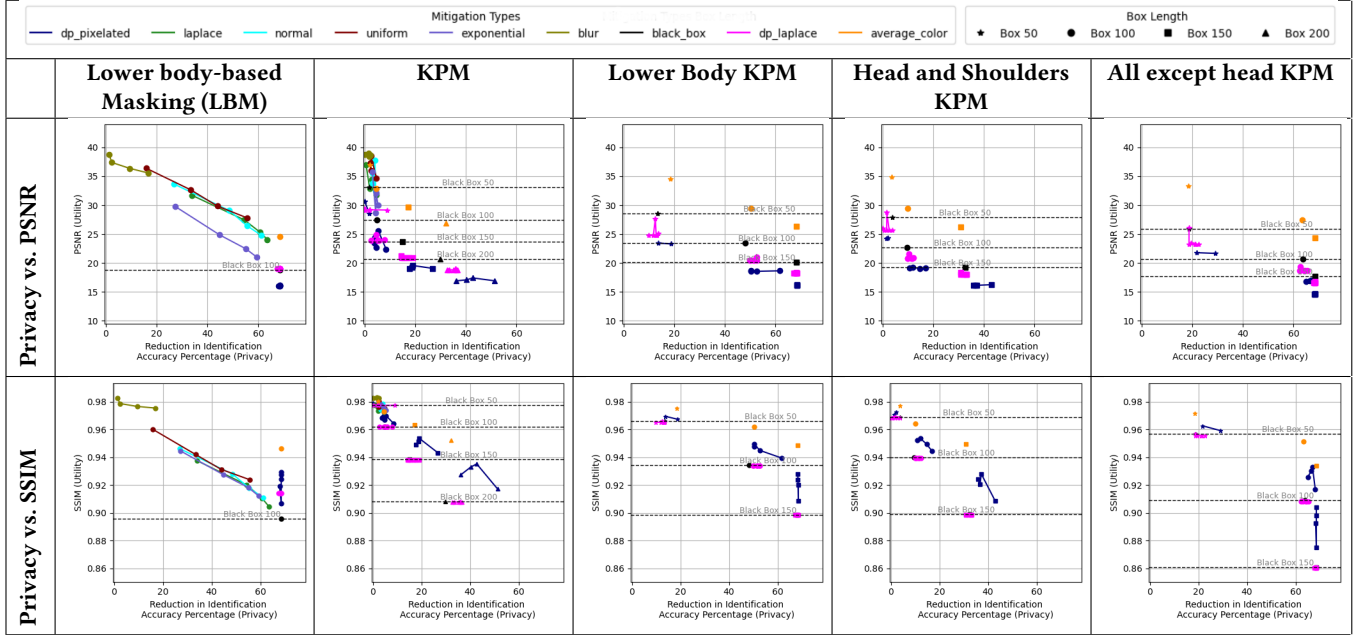
We summarize the privacy-utility tradeoff (PUT) of all the mitigation techniques in Table 1. Specifically, we focus on reducing user identification accuracy in percentage as a privacy metric (as explained in Section 5.3.2). This privacy metric was evaluated alongside two utility metrics: peak signal-to-noise ratio (PSNR), and structural similarity index measure (SSIM) as explained in Section 5.3.3.

6.3.1 Lower body mitigation (LBM). The results for the LBM approach can be seen in the first column of Table 1. The black box (baseline) achieved the maximum observed reduction in identification, 68%, with 18.8 PSNR and 0.90 SSIM.

Among the LBM mitigation techniques, blurring had the least capability to affect the identification accuracy with less than 17% reduction for all kernels. Additionally, results show that the random noise mitigation (Laplace, normal, uniform, and exponential) generally has close performance with better PSNR and SSIM than the black box but worse reduction in identification.

Furthermore, all block sizes *b* of DP pixelization and all ϵ of DP Laplace were able to achieve the same reduction in identification

Table 1: The privacy-utility tradeoff (PUT) of all mitigation techniques using gait features from the fully automated GaitExtract. The privacy metric (reduction in user identification accuracy) was compared with two different utility metrics: (1) PSNR and (2) SSIM.



as the black box, however, with a better SSIM than the black box. The average color also achieved the best SSIM of 0.946 and PSNR of 24.5 among the LBM mitigation techniques that achieved the maximum reduction in identification. This highlights that LBM effectively reduces an attacker’s ability to run an identification model by correlating the gait features to a user.

6.3.2 Keypoint mitigation (KPM). As seen in the second column of Table 1, blurring and random noises with *box_length* = 100 pixels performed poorly, having a reduction in the identification of less than 5%, which is much less than the black box, (baseline) performance of 13%. This suggests that random noises are ineffective mitigation techniques against identification attacks using gait features. In light of these results, the rest of the mitigation technique evaluations focus on DP pixelization (*DP-Pix*), *DP Laplace*, and average color compared to the black box.

Results show that *box_length* = 50, 100, 150 did not introduce a significant reduction in identification accuracy for the *DP-Pix*, *DP Laplace*, average color, and black box with most of the reduction being 11 – 20%. Significant reduction in identification accuracy only happens when increasing the *box_length* = 150 to 200, resulting in reductions greater than 30%. The largest drop in PSNR happens when increasing *box_length* = 50 to 100, with the drop in PSNR decreasing as the *box_length* increases. The opposite is true for SSIM, where the largest drop happens when increasing the *box_length* = 150 to 200.

DP pixelization had the highest reduction in identification, with better SSIM but worse PSNR than the black box. DP Laplace had a slightly better reduction in identification than the black box, with about the same PSNR and SSIM. Average color, on the other hand,

had a similar reduction in accuracy as the black box but much better SSIM and PSNR. These results show that KPM mitigation did not exhibit a favorable privacy-utility tradeoff compared with LBM, as most of the reduction in identification accuracy was less than 50%.

6.3.3 Lower body KPM. As seen in the third column of Table 1, lower body KPM was able to achieve the observed maximum reduction in identification accuracy, which was 68% with all mitigation types of *box_length* = 150.

Results show that the largest improvement in reduction of identification for all the mitigation types is observed when increasing *box_length* = 50 to *box_length* = 100 with an increase of 27 – 35%, at the cost of a drop in PSNR by 4.7 – 6.7 and a drop in SSIM by 0.03, except for average color, where the SSIM drops by 0.01.

Increasing *box_length* = 100 to 150 results in an increase of the privacy metric (reduction in identification accuracy) of 14 – 20% at the cost of a drop in PSNR of about 2.3 – 3.9 and a drop in SSIM of about 0.03, except for the average color, where the SSIM dropped about 0.01. The average color of *box_length* = 150 achieved the best privacy with only a slight decrease of PSNR of 3.1 and SSIM of 0.01. These results show that unlike KPM, lower body KPM significantly reduces an attacker’s ability to conduct an identification attack through gait features, highlighting the effectiveness of perturbing more keypoints.

6.3.4 Head and shoulders KPM. The fourth column of Table 1 shows that this approach introduced a higher identification accuracy reduction than the KPM approach with the same *box_length*.

Reduction in identification was smallest when increasing the *box_length* = 50 to 100 with an increase of 7.7 – 8.6% with the cost

of a drop of 5.1 – 5.3 in PSNR and 0.02 – 0.03 in SSIM. Increasing $box_length = 100$ to 150 doubled the increase in the reduction of identification accuracy with 13 – 17% at the cost of a drop of 2.9 – 3.4 in PSNR and 0.03 – 0.04 in SSIM. The average color’s performance also shows that increasing $box_length = 100$ to 150 only introduces an increase of 4% in the reduction of identification accuracy, at the cost of a drop in the PSNR by 3.15 and in the SSIM by 0.01. These results show that while the performance of this mitigation location was better than KPM, it still exhibits a unfavorable privacy-utility tradeoff compared to LBM and lower body KPM.

6.3.5 All except head KPM. This last column of Table 1 shows that this mitigation location has the most combinations that reached the observed maximum reduction in identification accuracy.

Most mitigation techniques had a greater than 60% reduction in identification accuracy with the worst SSIM and PSNR performance compared to the other KPM approaches. However, the DP pixelization results for this approach also show that after a certain point, increasing the box_length or $kernel_size$ does not introduce better privacy and degrades the utility. Particularly, the combination of DP pixelization with $box_length = 100$ and $kernel_size = 10$ achieved the best SSIM and PSNR with maximum reduction in identification accuracy.

Thus, for all except head KPM, the average color mitigation of $box_length = 100$ had the best privacy-utility trade-off, with a reduction of 63%, a PSNR of 27.4, and an SSIM of 0.951.

6.3.6 Key observations. Results show that among the keypoint-based approaches, mitigation applied at lower body KPM location with the average color mitigation type applied achieved the best privacy-utility tradeoff with the maximum reduction in identification accuracy of 68% and best PSNR and SSIM among all the techniques that achieved maximum privacy metric.

A close second is using LBM location with the average color mitigation type, which also achieved maximum reduction in identification accuracy and differing only in 1.8 for PSNR and 0.003 for SSIM compared to the lower body KPM. Across all the mitigation types, the average color showed the best privacy-utility tradeoff.

KPM results show that mitigating only the three keypoints used for gait feature extraction is insufficient because OpenPose uses other body parts to approximate the location of each keypoint. This is further exhibited in the head and shoulders KPM, where the privacy metric performance was better than KPM for similar box_length , exhibiting that mitigating additional keypoints not near the lower body improved privacy.

Another notable observation is that DP pixelization and the average color of LBM and DP pixelization and average color with $box_length = 150$ of lower body KPM performed similarly regarding privacy and utility. This is because choosing a large enough area for each of the keypoints on the lower body is almost equivalent to applying mitigation using lower body-based masking.

Comprehensive insights into the performance of each mitigation technique, along with the effects of the adjusted parameters (λ , b , c , box_length) on all privacy loss metrics (Jensen-Shannon Divergence (JSD) and user identification accuracy) and utility metrics (PSNR and SSIM) are available in Appendix F.

In summary, we conclude that by evaluating the 248 mitigation techniques, using lower body KPM with average color mitigation

type achieves the best privacy-utility tradeoff. However, we need to consider another utility tradeoff for real-time implementation: the system utility measured in latency and the fps as explained in Section 5.3.3. Hence, for the real-time implementation, we opt to choose the second best, which is LBM with (1) average color for its favorable PUT and (2) DP pixelization for its DP guarantees with second best PUT, as will be explained further in Section 7.

7 GAITGUARD SYSTEM DESIGN

We present the first-ever real-time implementation of a gait privacy protection system in mixed reality. Our system, referred to as **GaitGuard**, uses a multi-user collaborative application setup and is implemented on the mixed reality headset Hololens 2. Our proposed **GaitGuard** real-time prototype is shown in Figure 13 and further explained in this section.

All the evaluated mitigation techniques presented in Section 6 are feasible as offline defenses, such as enforcing gait privacy protection mechanisms before releasing videos. A prerequisite of keypoint-based masking mitigation is the use of pose estimation algorithms, such as OpenPose. However, benchmark frame rate (fps) results of OpenPose show that it is not appropriate for real-time defense as it was only able to achieve 11 fps with server-grade Nvidia V100 GPU and 0.1 fps when running on CPU only [23]. This performance of Openpose is much lower than the recommended streaming rate of 30 fps [5]. Thus, we limit our attention to lower body-based masking (LBM), which shows second-best PUT results as mentioned in Section 6.3.6. In the future, when pose estimation algorithms like OpenPose become faster, then keypoint-based masking defenses can also be integrated into real-time defenses.

As for the mitigation type, we evaluated real-time average color mitigation (the best in terms of PUT for LBM) and the real-time implementation of DP pixelization (the second best in terms of PUT for LBM) for DP guarantees.

Experiments also show that implementing the defense on-device introduces unacceptable latency; thus, we focus on mobile server-assisted design. On-device implementation details and results can be seen in Appendix G.

Accordingly, in this prototype we are targeting the threat model of server level and collaborative user attacks with any of the potential threat scenarios as explained in Section 3. To design a real-time implementation for device level or application level threat model, we need to use on-device implementation, which is currently infeasible.

7.1 Server Assisted Design with GaitGuard

An overview of **GaitGuard**’s trusted mobile server implementation with a collaborative application as shown in Figure 13. The flow of information begins with the Hololens unity app, where instead of sending the RGB camera frames to the network manager, it is intercepted and first sent to the trusted **GaitGuard** mobile server so that the frames received by the network manager are mitigated.

7.1.1 GaitGuard Design. **GaitGuard** employs two key functionalities to implement the mitigation. The first involves detecting the lower body of individuals within the camera frame, while the second entails applying the mitigation on the identified region. We

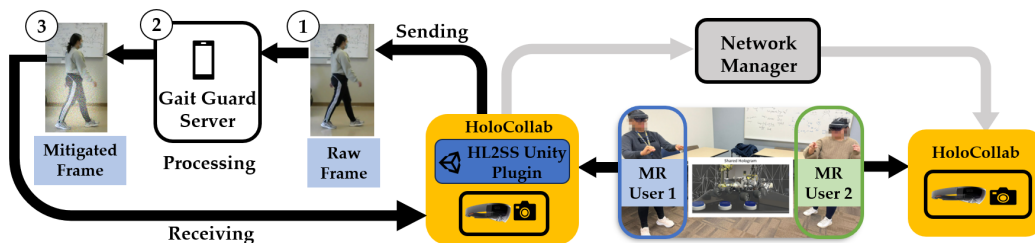


Figure 13: HoloCollab with GaitGuard Implementation. Raw camera frames are streamed from User 1’s HoloCollab to the GaitGuard server at 30 fps using the HL2SS Unity plugin. GaitGuard then processes the frames at a rate of 23.31 FPS and sends the mitigated frames back to User 1’s HoloCollab. User 1’s HoloCollab receives the mitigated frames at a rate of 23.18 fps.

discuss the implementation of DP pixelization and average color mitigation types with lower body-based masking (LBM).

Initially, **GaitGuard** identifies users in the frame and returns their locations through rectangular bounding boxes using OpenCV’s Histogram of Gradients (HOG) [15] default people detector with HOG’s pre-trained SVM classifier. Using this bounding box, we can approximate the boundaries of the lower body.

Afterward, **GaitGuard** applies the mitigation type, whether it is average color mitigation or DP pixelization to the identified area.

7.1.2 GaitGuard & HoloCollab Implementation. We designed a collaborative MR application, **HoloCollab**, to assess the effect of **GaitGuard** on the performance of a collaborative application. We built the application prototype in Unity 2021.3.25f1, using MRTK3, the third generation of Microsoft Mixed Reality Toolkit for Unity. Additionally, we used the Photon Unity Networking (PUN) 2 version 2.43 package to integrate multi-user functionality in the application. We used the Hololens 2 Sensor Streaming (HL2SS) [37] plugin to stream camera frames from the Hololens 2 to the **GaitGuard** local server. **GaitGuard** was implemented as a mobile server using Python and was written in ≈ 270 lines of code. The collaborative application was deployed on a Microsoft Hololens 2 device running Windows Holographic for Business Build 22621.1252.

7.1.3 System Evaluation. The recommended application frame rate for the Hololens 2 is 60 fps to ensure the best quality in user experiences [6]³. Moreover, it has been reported that the capability of streaming and recording frames from the RGB camera in Hololens 2 containing virtual objects, referred to as Mixed Reality Capture (MRC), has an average frame rate of 30 fps [5]. To evaluate the performance with **GaitGuard** on **HoloCollab**, we measured the system’s application frame rate and camera streaming frame rate.

The application frame rate of the **HoloCollab** without streaming is approximately 50 fps. Consequently, the application frame rate of **HoloCollab** when streaming camera frames to a vanilla server designed to ingest the frames simply dropped to 40 fps. We also observed that the application frame rate of **HoloCollab** with **GaitGuard** also resulted in 40 fps. This suggests that the decrease

in application frame rate was caused by the use of the HL2SS plugin and not by **GaitGuard**. Furthermore, this also implies that the **GaitGuard** local server does not affect the application frame rate.

We also report the camera streaming frame rate to identify **GaitGuard**’s effect on streaming latency. The average camera streaming fps at which the HL2SS plugin streams the camera frames is 30 fps, introducing latency of ≈ 33.33 ms at point number (1) in Figure 13. **GaitGuard** server then processes the camera frames at 23.31 fps, introducing latency of ≈ 42.90 ms at point number (2) in Figure 13. Finally, **GaitGuard** server then sends mitigated frames at a rate of 23.18 fps introducing latency of ≈ 43.14 ms at point number (3) in Figure 13. Hence, **GaitGuard** introduces a latency of 118.77 ms, which is the latency between point (1) and point (3) before the collaborative MR application sends the camera frames to the network manager.

We observed that either using average color or DP pixelization mitigation achieves comparable system utility in terms of latency, application fps, and streaming frame rate.

7.1.4 Qualitative Evaluation. We conducted a user study with 20 participants to understand and investigate perceptions of gait privacy. This comprised of a two-part survey: (1) initially gauging participants’ comfort with sharing unmodified frames and mitigated frames and (2) then assessing changes in their comfort after being informed of gait privacy concerns in MR and **GaitGuard**’s ability to reduce identification accuracy up to 68% and introducing a latency of 118 ms. The results of the survey are shown in Figure 14 using Likert scale [2]. The first part of the survey revealed a split in comfort levels, with 50% uncomfortable and 40% comfortable sharing unmodified frames with a slight increase to 65% in sharing mitigated frames.

The second part showed that awareness of privacy risks decreased the overall comfort in sharing unmodified frames but 75% felt more comfortable sharing mitigated frames as processed by **GaitGuard**. This highlights the importance of informed consent and awareness of privacy measures.

8 LIMITATIONS AND FUTURE WORK

The evaluation of the mitigation techniques was based on a dataset of 20 young adult individuals, and as such, it might be possible to

³Application frame rate is a metric that Microsoft uses to qualify the quality of their applications [3].

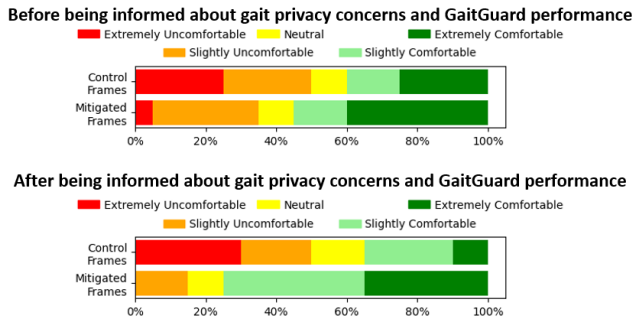


Figure 14: The distribution of Likert responses for the gait privacy perception survey across unmodified and mitigated frames with GaitGuard.

achieve better results for larger sample sizes. However, we have already shown the efficacy of the mitigation techniques on data from 20 people, and prior work has shown that evaluating anonymization techniques on smaller datasets makes for a more reliable evaluation [47]. Future studies can investigate the threat of identification through gait features in a more diverse population.

The present gait feature extraction framework, **GaitExtract**, has a limitation where if the user does not complete a gait cycle (two heel-strikes or two toe-offs) [58] in a walking sequence, then **GaitExtract** is unable to extract any gait features. Despite this, we have shown that identification through gait features is still feasible even when utilizing short distances of walking sequences (2.5m to 2.75m). This walking distance is a more appropriate emulation of real-world scenarios where MR spaces are typically constrained, limiting the distances that other MR users or bystanders can walk within the MR headset’s view.

Implementing **GaitGuard** at the OS level (on-device) is ideal for comprehensive protection. However, identification attacks through gait features at the OS level require pose estimation algorithms like Openpose to run on-device. Currently, pose estimation algorithms are not ported for MR headsets. Additionally, experiments have shown that running computationally heavy algorithms, such as person detection on a device, critically hinders the device’s functionality. OpenPose is significantly more demanding than person detection making it unfeasible. As MR technology evolves and real-time on-device pose estimation becomes feasible, the corresponding defense mechanisms will become feasible as well.

9 CONCLUSION

In this paper, we explored the state of gait privacy in MR applications by leveraging an automated gait extraction framework called **GaitExtract** and revealing that an attacker can collect gait information using minimal resources. We provided a comprehensive evaluation of possible mitigation techniques against identification using gait features. Furthermore, we developed **GaitGuard**, the first ever real-time implementation of a gait privacy protection in mixed reality. **GaitGuard**’s implementation as a mobile server of a collaborative application showed that it did not affect the application frame rate of the MR device and only introduced 118.77 ms

latency in streaming video frames. We believe that this work expands the understanding of gait privacy in MR applications and that our contribution is a step towards ensuring gait privacy of MR applications in the future.

ACKNOWLEDGEMENT

The authors used an academic version of ChatGPT4 provided by their academic institute to revise part of the text to “correct any typos, grammatical errors, and phrasing.” This research was partially supported by NSF award # CNS-2105084, NSF award 1956393, and a gift from the Noyce Initiative.

REFERENCES

- [1] 2013. The CPRA. <https://thecpra.org/>.
- [2] 2018. Likert Scale: Definition, Examples & How to Use It. <https://www.questionpro.com/blog/what-is-likert-scale/>.
- [3] 2022. App Quality Criteria - Mixed Reality. <https://learn.microsoft.com/en-us/windows/mixed-reality/develop/advanced-concepts/app-quality-criteria-overview>.
- [4] 2022. Introduction to the Multi-user Capabilities Tutorials - Mixed Reality. <https://learn.microsoft.com/en-us/windows/mixed-reality/develop/unity/tutorials/mr-learning-sharing-01>.
- [5] 2022. Mixed Reality Capture Overview. <https://learn.microsoft.com/en-us/windows/mixed-reality/develop/advanced-concepts/mixed-reality-capture-overview>.
- [6] 2022. Performance - MRTK 2. <https://learn.microsoft.com/en-us/windows/mixed-reality/mrtk-unity/mrtk2/performance/perf-getting-started?view=mrtkunity-2022-05>.
- [7] 2023. Apple Vision Pro. <https://www.apple.com/apple-vision-pro/>.
- [8] 2023. Bouvet. <https://www.microsoft.com/en-us/p/lens-by-bouvet/9p29ft8z34zs>.
- [9] 2023. Catapult Mixed Reality Client and Development Application. <https://www.makesea.com/download/>.
- [10] 2023. General Data Protection Regulation (GDPR). <https://gdpr-info.eu/>.
- [11] 2023. HoloLens Microsoft 2. <https://www.microsoft.com/en-us/hololens/>.
- [12] 2023. HoloLens2ForCV. <https://github.com/microsoft/HoloLens2ForCV/tree/main/Samples/CameraWithCVAndCalibration>.
- [13] 2023. Meta Quest 3: Mixed Reality VR Headset. <https://www.meta.com/quest/quest-3/>.
- [14] 2023. Microsoft Apps. <https://apps.microsoft.com/home?hl=en-US&gl=US>.
- [15] 2023. OpenCV. https://docs.opencv.org/3.4/d5/d33/struct_cv_1_1HOGDescriptor.html.
- [16] 2023. Overview of Dynamics 365 Remote Assist on HoloLens and HoloLens 2. <https://learn.microsoft.com/en-us/dynamics365/mixed-reality/remote-assist/overview-hololens>.
- [17] 2023. Photon Unity Networking for Unity Multiplayer Games PUN2. <https://www.photonengine.com/PUN>.
- [18] 2023. Pose Estimation. <https://paperswithcode.com/task/pose-estimation>.
- [19] 2023. Sklearn.Ensemble.GradientBoostingClassifier. <https://scikit-learn.org/stable/modules/generated/sklearn.ensemble.GradientBoostingClassifier.html>.
- [20] 2023. Sphere XR. <https://apps.microsoft.com/detail/9P11TRNWG2HR?hl=en-US>.
- [21] 2023. What Is Mixed Reality? <https://learn.microsoft.com/en-us/windows/mixed-reality/discover/mixed-reality>.
- [22] 2024. Blur your videos - YouTube Help. <https://support.google.com/youtube/answer/9057652?hl=en>.
- [23] 2024. OpenPose: OpenPose Doc - Maximizing the OpenPose Speed. https://cmu-perceptual-computing-lab.github.io/openpose/web/html/doc/md_doc_06_maximizing_openpose_speed.html.
- [24] 2024. Structural Similarity Index - NI. https://www.ni.com/docs/en-US/bundle/ni-vision-concepts-help/page/structural_similarity_index.html.
- [25] Duin Baek, Pratik Musale, and Jihoon Ryou. 2019. Walk to show your identity: gait-based seamless user authentication framework using deep neural network. In *The 5th ACM Workshop on Wearable Systems and Applications*. 53–58.
- [26] Fahimeh Bahmaninezhad, Chunlei Zhang, and John Hansen. 2018. Convolutional Neural Network Based Speaker De-Identification. 255–260. <https://doi.org/10.21437/Odyssey.2018-36>
- [27] Richard Baker, Alberto Esquenazi, Maria Grazia Benedetti, Kaat Desloovere, et al. 2016. Gait analysis: clinical facts. *Eur. J. Phys. Rehabil. Med* 52, 4 (2016), 560–574.
- [28] Zhe Cao, Tomas Simon, Shih-En Wei, and Yaser Sheikh. 2017. Realtime multi-person 2d pose estimation using part affinity fields. In *Proceedings of the IEEE conference on computer vision and pattern recognition*. 7291–7299.
- [29] Aurelio Cappozzo. 1984. Gait analysis methodology. *Human movement science* 3, 1-2 (1984), 27–50.
- [30] Kaiming Cheng, Jeffery F Tian, Tadayoshi Kohno, and Franziska Roesner. 2023. Exploring user reactions and mental models towards perceptual manipulation attacks in mixed reality. In *USENIX Security*, Vol. 18.
- [31] Guglielmo Cola, Marco Avvenuti, Fabio Musso, and Alessio Vecchio. 2016. Gait-based authentication using a wrist-worn device. In *Proceedings of the 13th International Conference on Mobile and Ubiquitous Systems: Computing, Networking and Services*. 208–217.
- [32] Matthew Corbett, Brendan David-John, Jiacheng Shang, Y Charlie Hu, and Bo Ji. 2023. BystanderAR: Protecting Bystander Visual Data in Augmented Reality Systems. In *Proceedings of the 21st Annual International Conference on Mobile Systems, Applications and Services*. 370–382.
- [33] Paula Delgado-Santos, Ruben Tolosana, Richard Guest, Ruben Vera-Rodriguez, Farzin Deravi, and Aythami Morales. 2022. GaitPrivacyON: Privacy-preserving mobile gait biometrics using unsupervised learning. *Pattern Recognition Letters* 161 (Sept. 2022), 30–37. <https://doi.org/10.1016/j.patrec.2022.07.015>
- [34] Paula Delgado-Santos, Ruben Tolosana, Richard Guest, Ruben Vera-Rodriguez, Farzin Deravi, and Aythami Morales. 2022. GaitPrivacyON: Privacy-preserving mobile gait biometrics using unsupervised learning. *Pattern Recognition Letters* 161 (2022), 30–37.
- [35] Lucie Denisart, Diana Zapata-Dominguez, Xavier David, Aubin Leclere, Romain Lelong, Chaoyue Liu, Jiahui Xu, Emilie Loup-Escande, and Alejandro A. Franco. 2024. Combining Virtual Reality with Mixed Reality for Efficient Training in Battery Manufacturing. *Batteries & Supercaps* 7, 1 (2024), e202300268. <https://doi.org/10.1002/batt.202300268>
- [36] Mohammad O Derawi, Patrick Bours, and Kjetil Holien. 2010. Improved cycle detection for accelerometer based gait authentication. In *2010 Sixth International Conference on Intelligent Information Hiding and Multimedia Signal Processing*. IEEE, 312–317.
- [37] Juan C Dibene and Enrique Dunn. 2022. HoloLens 2 Sensor Streaming. *arXiv preprint arXiv:2211.02648* (2022).
- [38] Liyue Fan. 2018. Image pixelization with differential privacy. In *Data and Applications Security and Privacy XXXII: 32nd Annual IFIP WG 11.3 Conference, DBSec 2018, Bergamo, Italy, July 16–18, 2018, Proceedings 32*. Springer, 148–162.
- [39] Habiba Farrukh, Reham Mohamed, Aniket Nare, Antonio Bianchi, and Z Berkay Celik. 2023. {LocIn}: Inferring Semantic Location from Spatial Maps in Mixed Reality. In *32nd USENIX Security Symposium (USENIX Security 23)*. 877–894.
- [40] Yu Fu, Yan Hu, and Veronica Sundstedt. 2022. A Systematic Literature Review of Virtual, Augmented, and Mixed Reality Game Applications in Healthcare. *ACM Transactions on Computing for Healthcare* 3, 2 (March 2022), 22:1–22:27. <https://doi.org/10.1145/3472303>
- [41] Moshe Gabel, Ran Gilad-Bachrach, Erin Renshaw, and Assaf Schuster. 2012. Full body gait analysis with Kinect. In *2012 Annual International Conference of the IEEE Engineering in Medicine and Biology Society*. IEEE, 1964–1967.
- [42] Davronzhon Gafurov, Kirsi Helkala, and Torjel Sondrol. 2006. Biometric Gait Authentication Using Accelerometer Sensor. *J. comput.* 1, 7 (2006), 51–59.
- [43] Davronzhon Gafurov, Einar Snekkenes, and Patrick Bours. 2007. Gait authentication and identification using wearable accelerometer sensor. In *2007 IEEE workshop on automatic identification advanced technologies*. IEEE, 220–225.
- [44] Jaris Gerup, Camilla B. Soerensen, and Peter Dieckmann. 2020. Augmented reality and mixed reality for healthcare education beyond surgery: an integrative review. 11 (Jan. 2020), 1–18. <https://doi.org/10.5116/ijme.5e01eb1a>
- [45] Mar Gonzalez-Franco, Rodrigo Pizarro, Julio Cermeron, Katie Li, Jacob Thorn, Windo Hutabarat, Ashutosh Tiwari, and Pablo Bermell-Garcia. 2017. Immersive Mixed Reality for Manufacturing Training. *Frontiers in Robotics and AI* 4 (Feb. 2017). <https://doi.org/10.3389/frobt.2017.00003> Publisher: Frontiers.
- [46] Sindhu Reddy Kalathur Gopal, Diksha Shukla, James David Wheelock, and Nitesh Saxena. 2023. Hidden reality: caution, your hand gesture inputs in the immersive virtual world are visible to all!. In *32nd USENIX Security Symposium (USENIX Security 23)*. 859–876.
- [47] Simon Hanisch, Julian Todt, Jose Patino, Nicholas Evans, and Thorsten Strufe. 2024. A False Sense of Privacy: Towards a Reliable Evaluation Methodology for the Anonymization of Biometric Data. *Proceedings on Privacy Enhancing Technologies* (2024).
- [48] C.E. Hughes, C.B. Stapleton, D.E. Hughes, and E.M. Smith. 2005. Mixed reality in education, entertainment, and training. *IEEE Computer Graphics and Applications* 25, 6 (Nov. 2005), 24–30. <https://doi.org/10.1109/MCG.2005.139> Conference Name: IEEE Computer Graphics and Applications.
- [49] Ismat Jarin, Yu Duan, Rahmadi Trimananda, Hao Cui, Salma Elmalaki, and Athina Markopoulou. 2023. BehaVR: User Identification Based on VR Sensor Data. *arXiv preprint arXiv:2308.07304* (2023).
- [50] Sudhakar Kumawat and Hajime Nagahara. 2022. Privacy-Preserving Action Recognition via Motion Difference Quantization. In *European Conference on Computer Vision*. Springer, 518–534.
- [51] Kiron Lebeck, Kimberly Ruth, Tadayoshi Kohno, and Franziska Roesner. 2018. Towards security and privacy for multi-user augmented reality: Foundations with end users. In *2018 IEEE Symposium on Security and Privacy (SP)*. IEEE, 392–408.
- [52] Rationalstat LLC. 2023. Mixed Reality Market Is Set to Double by 2030 | Mixed Reality Market Share, Size, Growth, Forecast, 2023-2030 | RationalStat Study. <https://www.globenewswire.com/news-release/2023/09/22/2747789/0/en/Mixed-Reality-Market-is-Set-to-Double-by-2030-Mixed-Reality-Market-Share-Size-Growth-Forecast-2023-2030-RationalStat-Study.html>.
- [53] Luca Lonini, Yaejin Moon, Kyle Embry, R James Cotton, Kelly McKenzie, Sophia Jenz, and Arun Jayaraman. 2022. Video-based pose estimation for gait analysis in stroke survivors during clinical assessments: a proof-of-concept study. *Digital Biomarkers* 6, 1 (2022), 9–18.
- [54] Melanie J. Maas and Janette M. Hughes. 2020. Virtual, augmented and mixed reality in K–12 education: a review of the literature. *Technology, Pedagogy and Education* 29, 2 (March 2020), 231–249. <https://doi.org/10.1080/1475939X.2020.1737210>
- [55] Meta. 2024. Introducing Project Aria from Meta. <https://www.projectaria.com3> [Online; accessed 21-Feb-2024].
- [56] Muhammad Muaz and Rene Mayrhofer. 2014. Orientation independent cell phone based gait authentication. In *Proceedings of the 12th International Conference on Advances in Mobile Computing and Multimedia*. 161–164.

- [57] Musculoskeletal Key. 2024. Gait. https://musculoskeletalkey.com/18-gait/#c018_f002 [Online; accessed 28-Feb-2024].
- [58] Anup Nandy, Saikat Chakraborty, Jayeeta Chakraborty, and Gentiane Venture. 2021. *Modern methods for affordable clinical gait analysis: theories and applications in healthcare systems*. Academic Press.
- [59] Ion P Pappas, Milos R Popovic, Thierry Keller, Volker Dietz, and Manfred Morari. 2001. A reliable gait phase detection system. *IEEE Transactions on neural systems and rehabilitation engineering* 9, 2 (2001), 113–125.
- [60] Alexandra Pfister, Alexandre M West, Shaw Bronner, and Jack Adam Noah. 2014. Comparative abilities of Microsoft Kinect and Vicon 3D motion capture for gait analysis. *Journal of medical engineering & technology* 38, 5 (2014), 274–280.
- [61] Hari Prasanth, Miroslav Caban, Urs Keller, Grégoire Courtine, Auke Ijspeert, Heike Vallery, and Joachim Von Zitzewitz. 2021. Wearable sensor-based real-time gait detection: A systematic review. *Sensors* 21, 8 (2021), 2727.
- [62] Kristina Prokopetc and Romain Dupont. 2019. Towards Dense 3D Reconstruction for Mixed Reality in Healthcare: Classical Multi-View Stereo vs Deep Learning. In *Proceedings of the IEEE/CVF International Conference on Computer Vision (ICCV) Workshops*.
- [63] Sanka Rasnayaka and Terence Sim. 2020. Your Tattletale Gait Privacy Invasiveness of IMU Gait Data. In *2020 IEEE International Joint Conference on Biometrics (IJCB)*. 1–10. <https://doi.org/10.1109/IJCB48548.2020.9304922> ISSN: 2474-9699.
- [64] Derek Reilly, Mohamad Salimian, Bonnie MacKay, Niels Mathiasen, W Keith Edwards, and Juliano Franz. 2014. SecSpace: prototyping usable privacy and security for mixed reality collaborative environments. In *Proceedings of the 2014 ACM SIGCHI symposium on Engineering interactive computing systems*. 273–282.
- [65] Zhiqi Shen, Shaojing Fan, Yongkang Wong, Tian-Tsong Ng, and Mohan Kankanhalli. 2019. Human-imperceptible Privacy Protection Against Machines. In *Proceedings of the 27th ACM International Conference on Multimedia (MM '19)*. Association for Computing Machinery, New York, NY, USA, 1119–1128. <https://doi.org/10.1145/3343031.3350963>
- [66] Warit Sirichotedumrong and Hitoshi Kiya. 2021. A gan-based image transformation scheme for privacy-preserving deep neural networks. In *2020 28th European Signal Processing Conference (EUSIPCO)*. IEEE, 745–749.
- [67] Olumide Sofuwa, Alice Nieuwboer, Kaat Desloovere, Anne-Marie Willems, Fabienne Chavret, and Ilse Jonkers. 2005. Quantitative gait analysis in Parkinson's disease: comparison with a healthy control group. *Archives of physical medicine and rehabilitation* 86, 5 (2005), 1007–1013.
- [68] Jan Stenum, Cristina Rossi, and Ryan T Roemmich. 2021. Two-dimensional video-based analysis of human gait using pose estimation. *PLoS computational biology* 17, 4 (2021), e1008935.
- [69] Mojtaba Taherisadr, Mohammad Abdullah Al Faruque, and Salma Elmalaki. 2023. Erudite: Human-in-the-loop iot for an adaptive personalized learning system. *IEEE Internet of Things Journal* (2023).
- [70] Ngoc-Dung T. Tieu, Huy H. Nguyen, Fuming Fang, Junichi Yamagishi, and Isao Echizen. 2019. An RGB Gait Anonymization Model for Low-Quality Silhouettes. In *2019 Asia-Pacific Signal and Information Processing Association Annual Summit and Conference (APSIPA ASC)*. 1686–1693. <https://doi.org/10.1109/APSIPAASC47483.2019.9023188>
- [71] Christopher L Vaughan. 2003. Theories of bipedal walking: an odyssey. *Journal of biomechanics* 36, 4 (2003), 513–523.
- [72] Keiichi Watanuki. 2011. A Mixed Reality-based Emotional Interactions and Communications for Manufacturing Skills Training. In *Emotional Engineering: Service Development*, Shuichi Fukuda (Ed.). Springer, London, 39–61. https://doi.org/10.1007/978-1-84996-423-4_3
- [73] Chengshuo Xia, Atsuya Munakata, and Yuta Sugiura. 2023. Privacy-Aware Gait Identification With Ultralow-Dimensional Data Using a Distance Sensor. *IEEE Sensors Journal* 23, 9 (May 2023), 10109–10117. <https://doi.org/10.1109/JSEN.2023.3260846> Conference Name: IEEE Sensors Journal.
- [74] Weitao Xu, Guohao Lan, Qi Lin, Sara Khalifa, Mahbub Hassan, Neil Bergmann, and Wen Hu. 2019. KEH-Gait: Using Kinetic Energy Harvesting for Gait-based User Authentication Systems. *IEEE Transactions on Mobile Computing* 18, 1 (Jan. 2019), 139–152. <https://doi.org/10.1109/TMC.2018.2828816> Conference Name: IEEE Transactions on Mobile Computing.
- [75] Weitao Xu, Yiran Shen, Yongtuo Zhang, Neil Bergmann, and Wen Hu. 2017. Gait-Watch: A Context-aware Authentication System for Smart Watch Based on Gait Recognition. In *Proceedings of the Second International Conference on Internet-of-Things Design and Implementation (IoTDI '17)*. Association for Computing Machinery, New York, NY, USA, 59–70. <https://doi.org/10.1145/3054977.3054991>
- [76] Shiqi Yu, Tieniu Tan, Kaiqi Huang, Kui Jia, and Xinyu Wu. 2009. A study on gait-based gender classification. *IEEE Transactions on image processing* 18, 8 (2009), 1905–1910.
- [77] Michał Zajac, Konrad Zolna, Negar Rostamzadeh, and Pedro O Pinheiro. 2019. Adversarial framing for image and video classification. In *Proceedings of the AAAI Conference on Artificial Intelligence*, Vol. 33. 10077–10078.
- [78] De Zhang, Yunhong Wang, and Bir Bhanu. 2010. Ethnicity classification based on gait using multi-view fusion. In *2010 IEEE Computer Society Conference on Computer Vision and Pattern Recognition-Workshops*. IEEE, 108–115.
- [79] Yicheng Zhang, Carter Slocum, Jiasi Chen, and Nael Abu-Ghazaleh. 2023. It's all in your head (set): Side-channel attacks on ar/vr systems. In *USENIX Security*.
- [80] Yuhan Zhou, Robbin Romijnders, Clint Hansen, Jos van Campen, Walter Maetzler, Tibor Hortobágyi, and Claudine JC Lamoth. 2020. The detection of age groups by dynamic gait outcomes using machine learning approaches. *Scientific reports* 10, 1 (2020), 4426.

APPENDIX

A GAIT FEATURES

Figure 15 shows a visual representation of the different gait features, including step time, stance time, swing time, and double support time, that form the gait cycle [57, 58].

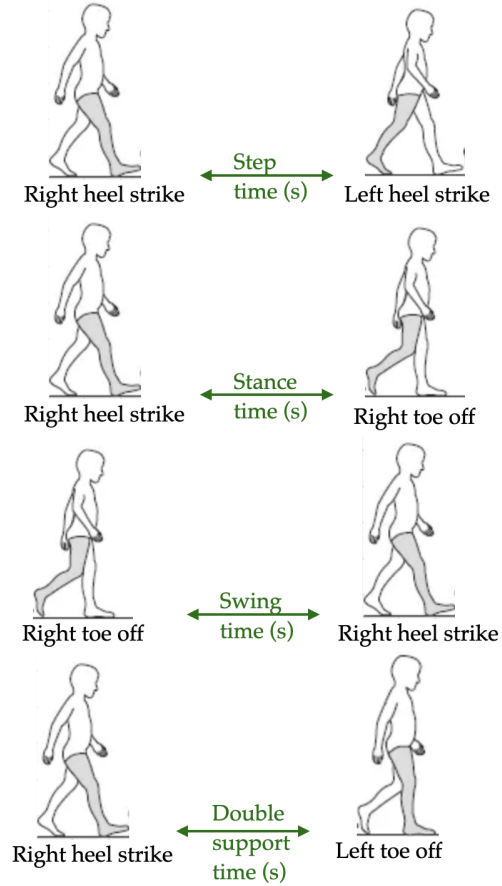


Figure 15: Different gait features that form the gait cycle referenced with reference to the right leg [57].

B IDENTIFICATION MODEL COMPARISON

In Section 4.3, we discuss the capability of gait features extracted using **GaitExtract** in identifying people. In this appendix, we present the performance of different classifiers that identify people through gait features.

We compare different classifiers from the `scikit-learn` library in Python to observe which model performs the best in identifying individuals through gait features. We deliberately use already available models from the `scikit-learn` library to showcase that

easily accessible off-the-shelf models can identify people, highlighting that an adversary can easily execute an attack. As mentioned in Section 4.3.2, the amount of gait feature vectors produced by **GaitExtract** varied among each participants. Thus, we compare 10 different classifiers using data augmented through random over-sampling. Results are summarized in Table 2.

Table 2: Comparing the performance of classifiers in identifying people through gait features extracted using partially automated GaitExtract- using step length

Classifier	F1 Score
SVM	77.27%
KNN	73.28%
GradientBoost	91.66%
Random Forest	91.58%
Decision Tree	86.33%
MLP (64,3)	74.97%
MLP (128,3)	78.72%
MLP (1024,3)	83.75%
SGD classifier SVM	26.98%
Extra Trees	91.59%

We applied stratified cross-validation with 3-folds for each classifier and repeated the cross-validation 2 times to train each classifier. We used stratification to address the class imbalances among the number of extracted features. Cross-validation with 3-fold was used to ensure that an ample amount of testing data was still included even for classes with few features. Furthermore, we trained each classifier using gait features from the partially automated **GaitExtract** to observe its capability to identify people uniquely. We used the mean of weighted F1 scores across all folds to quantify classification accuracy. Results show that **GradientBoostClassifier** performed the best with 91.66%.

C NOISE PROBABILITY DISTRIBUTIONS

We investigate the following random noises in our mitigation techniques.

- Uniform noise distribution (\mathcal{U}): Generates noise with a uniform distribution, represented as $\mathcal{U}(-\lambda, \lambda)$. In this distribution, all values within the specified range are equally likely with probability density function (PDF): $f(x) = \frac{1}{2\lambda}$, where $x \in [-\lambda, \lambda]$.
- Normal noise distribution (\mathcal{N}): Characterized by a normal distribution, denoted as $\mathcal{N}(0, \lambda)$, centered at 0, and introducing variations with a standard deviation of λ . Hence, the PDF: $f(x) = \frac{1}{\sqrt{2\pi}\lambda} \cdot e^{-\frac{x^2}{2\lambda^2}}$ for $x \in (-\infty, \infty)$.
- Laplace noise distribution (\mathcal{L}): Generates noise with a Laplace distribution, expressed as $\mathcal{L}(0, \lambda)$, centered at 0, and with the scale parameter set to λ . Hence, the PDF: $f(x) = \frac{1}{2\lambda} \cdot e^{-\frac{|x|}{\lambda}}$ for $x \in (-\infty, \infty)$.
- Exponential noise distribution (\mathcal{E}): Generates noise with an exponential distribution, denoted by $\mathcal{E}(\lambda)$, where the rate parameter is set to λ . Hence, the PDF: $f(x) = \lambda \cdot e^{-\lambda x}$ for $x \geq 0$.

D WEAK VS. STRONG ADVERSARY

In Section 6 we focus on presenting the performance of the different mitigation techniques against a strong adversary. In this appendix, we compare a weak and strong adversary. As seen in Table 3, we focus on comparing how the reduction in identification accuracy differs between the two adversaries. More mitigation techniques reached the maximum reduction in identification when using a weak adversary model. For example, if an adversary is trained on clean frames and then mitigation technique DP-pixelization on **KPM** with the kernel $b = 10$ and $box_length = 150$ is applied, the reduction in identification accuracy compared to no mitigation is 25% on average.

E DISTRIBUTION OF GAIT FEATURES WITH VARIOUS MITIGATION TECHNIQUES

This appendix shows and discusses the JSD scores across all the mitigation techniques. The change in the distribution of each gait feature as measured by the average JSD is illustrated as a heatmap in Figure 16. The heatmaps follow the range of (0.14, 0.67). Lower JSD scores indicate that the mitigation technique was unsuccessful in changing the distribution, while higher JSD scores indicate a more significant change in the gait feature distribution.

As mentioned in Section 6.2, **KPM** had the lowest JSD scores as seen in Figure 11. The next approach that had the second to the least effect in shifting the distribution is the “**head and shoulders KPM**”. Figure 16a shows that most of its JSD values are less than 0.55, reinforcing the theory that OpenPose uses the relative locations of the other keypoints, in this case, the shoulder and head, to find the position of the midhip and ankle keypoints accurately.

Notably, the JSD scores for “**lower body KPM**” which was between 0.525 and 0.67, similar to the “**all except head KPM**” which was between 0.58 and 0.67. This is observed in Figures 12 (repeated here in the appendix as Figure 16b for convenience) and 16c where the heatmaps have similar intensities, indicating that adding more keypoints to mitigate does not translate to a linear shift in gait features distribution.

However, for the “**lower body-based masking (LBM)**” location that does not depend on the position of the keypoints, the JSD score is more dependent on the type of mitigation technique with DP pixelization, DP Laplace, and average color perturbation having the highest JSD scores in LBM with values ranging between 0.35 to 0.63 on average.

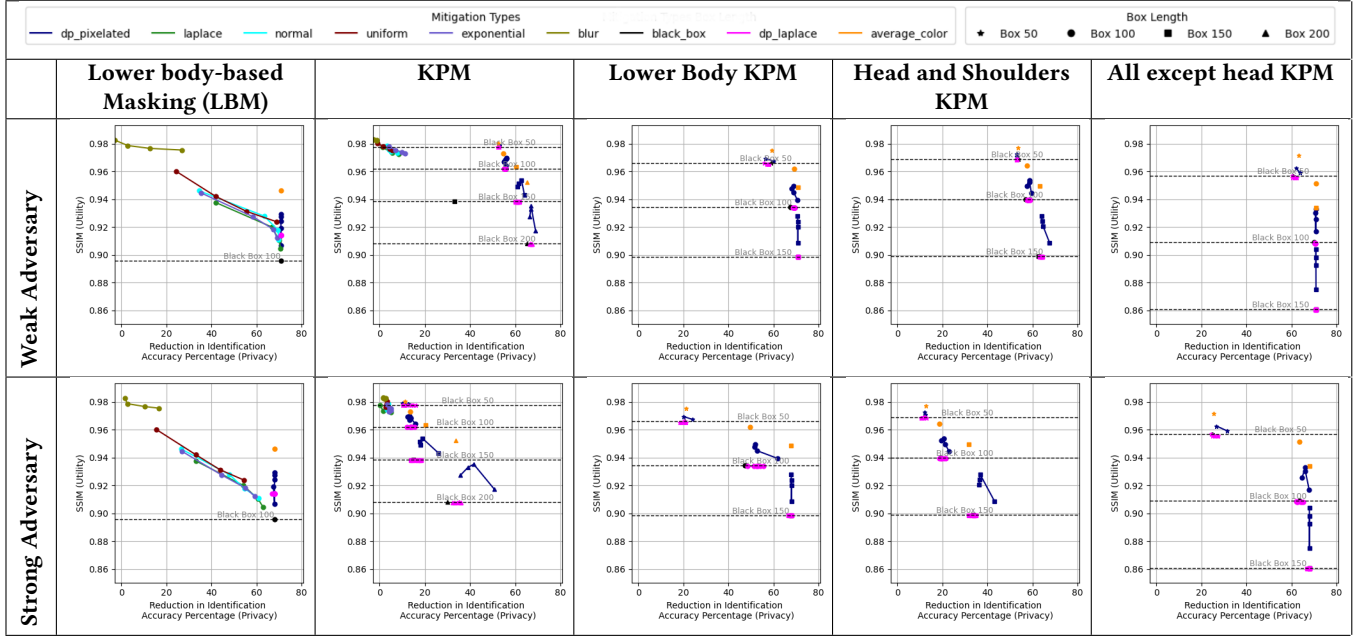
F PRIVACY AND UTILITY METRICS ACROSS VARIOUS MITIGATIONS

In Section 6.3, we evaluated the effect of the different mitigation techniques by focusing on the reduction of identification accuracy and its impact on the PSNR and SSIM utility metrics. In this appendix, we present the effect of different parameters against all the privacy and utility metrics discussed in Section 5.3.2.

F.1 Inter-type parameter effect

Table 4 shows the effect of parameters of different mitigation types against all the privacy (Average JSD, Reduction in Identification Accuracy) and utility metrics (SSIM, PSNR). The left column presents the values for the KPM approach, while the right column presents the values for the LBM approach.

Table 3: Weak vs Strong Adversary results.



- **Random noise parameter λ .** The KPM approach results show no relationship between λ and the JSD and a reduction in identification accuracy. A small positive correlation exists between λ and the average JSD values for all the noise distributions of LBM approach. Experiments show minimal improvement in privacy mitigation after $\lambda = 150$. Results show that increasing λ consistently decreases utility, but increasing λ only increases privacy for the LBM approach.
- **DP-Pix parameter b .** The size of the pixelization kernel b was varied for the DP-Pix mitigation. The effects of this parameter are summarized in the second row or Table 4. Results show that increasing b generally increases SSIM, but there is no strong trend for the PSNR, average JSD, or reduction in the identification metric. Pixelization kernel of size $b = 10$ commonly yields the highest reduction in identification accuracy.
- **DP Laplace parameter ϵ .** The results of varying ϵ for the DP Laplace is seen in the third row of Table 4. Results show no correlation with the privacy and utility metrics as ϵ increases.
- **Blur parameter c .** Increasing the blurring kernel using the KPM approach does not have any correlation with any of the privacy and utility metrics. While increasing the blurring kernel for the LBM approach shows a small positive correlation for the privacy metrics and a small negative correlation for the utility metrics. Blurring's privacy performance is lacking with JSD values less than 0.5 and a reduction in the identification of less than 20%.

In summary, varying the parameter for DP-Pix, DP Laplace didn't show a significant trend. This suggests that mitigation locations matter more for these types. Results also show that varying the parameters for the random noises and blurring only exhibits a significant correlation for the LBM granularity. These results suggest that other mitigation parameters, such as mitigation location, affect the utility and privacy metrics more.

F.2 Box length effect

Table 5 shows the effect of varying the size of the boxes for the different KPM approaches against the different privacy and utility metrics. As seen in the first column and second column of the table, increasing the `box_length` decreases the utility as measured by the SSIM and PSNR. Another notable observation is that increasing `box_length` shows a correlation with a higher reduction in identification accuracy for KPM and "head and shoulders KPM". However, the same relationship isn't observed for "lower body KPM" and "all except head KPM". Results show that the latter mitigation locations, even at smaller `box_lengths`, can achieve higher reduction values in identification and JSD. This indicates that "lower body KPM" and "all except head KPM" are better mitigation locations because achieving higher privacy metrics at smaller `box_length` results in better utility metrics.

G ON-DEVICE IMPLEMENTATION OF GAITGUARD

Proposed System Implementation. The first core functionality of GaitGuard, which is identifying the lower body area in the frame, suggests that there is a need for a real-time and on-device solution to detect the lower body of a person. As discussed in section 7.1.1, the proposed implementation of this functionality is to use OpenCV's HOG default person detector and SVM classifier. To implement OpenCV on the HoloLens, we exploited OpenCV library that Microsoft provides as part of their HoloLens2ForCV project [12]. The third-party application containing the core functionality of GaitGuard was completed in C++. An overview of this on-device implementation can be seen in Figure 17.

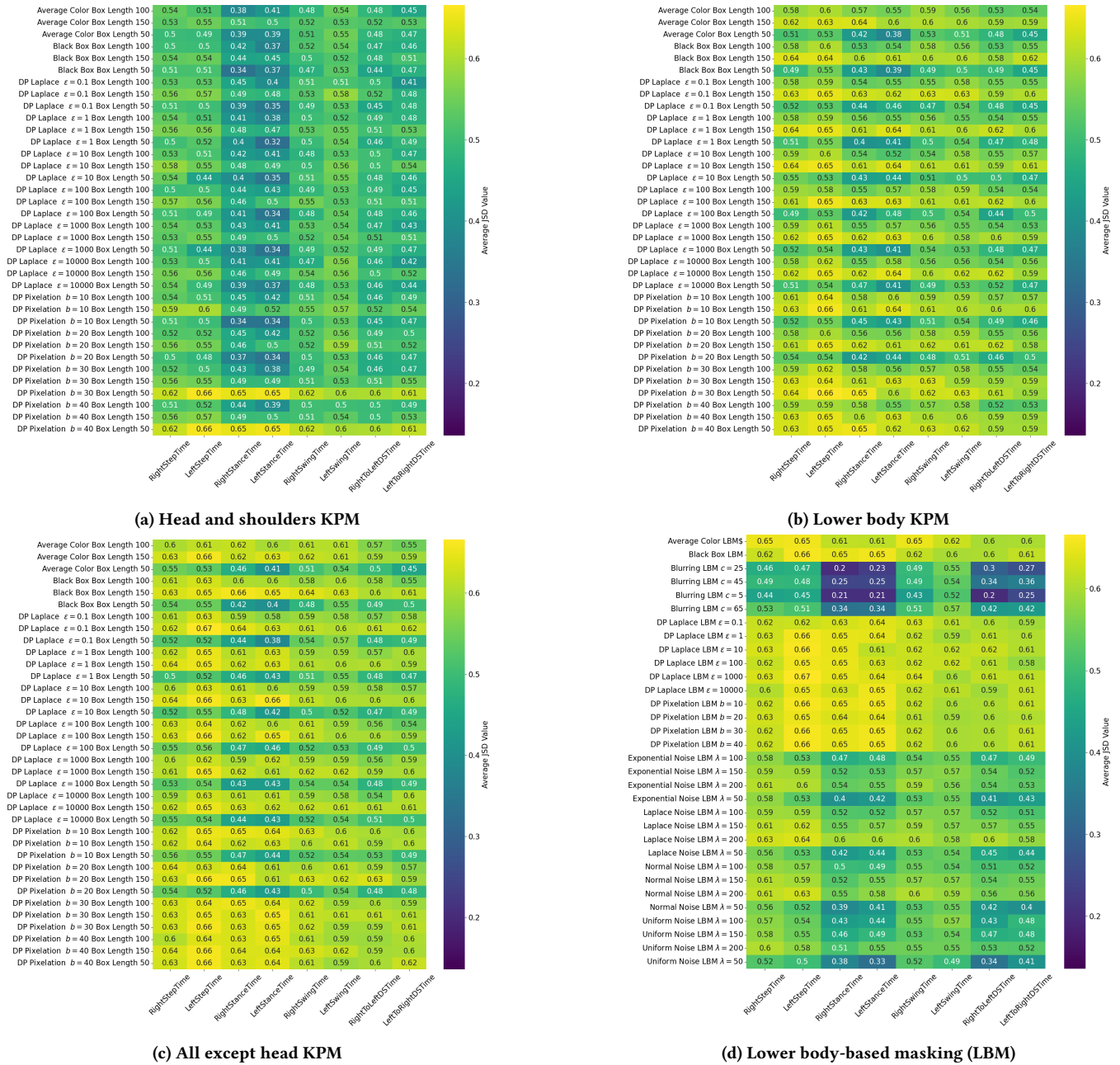


Figure 16: JSD Heatmaps across various mitigation techniques.

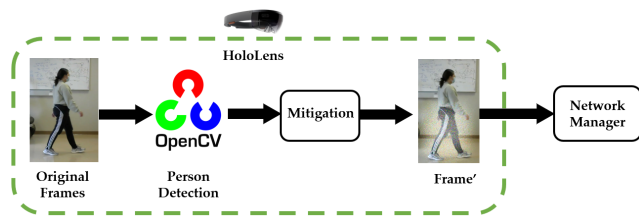
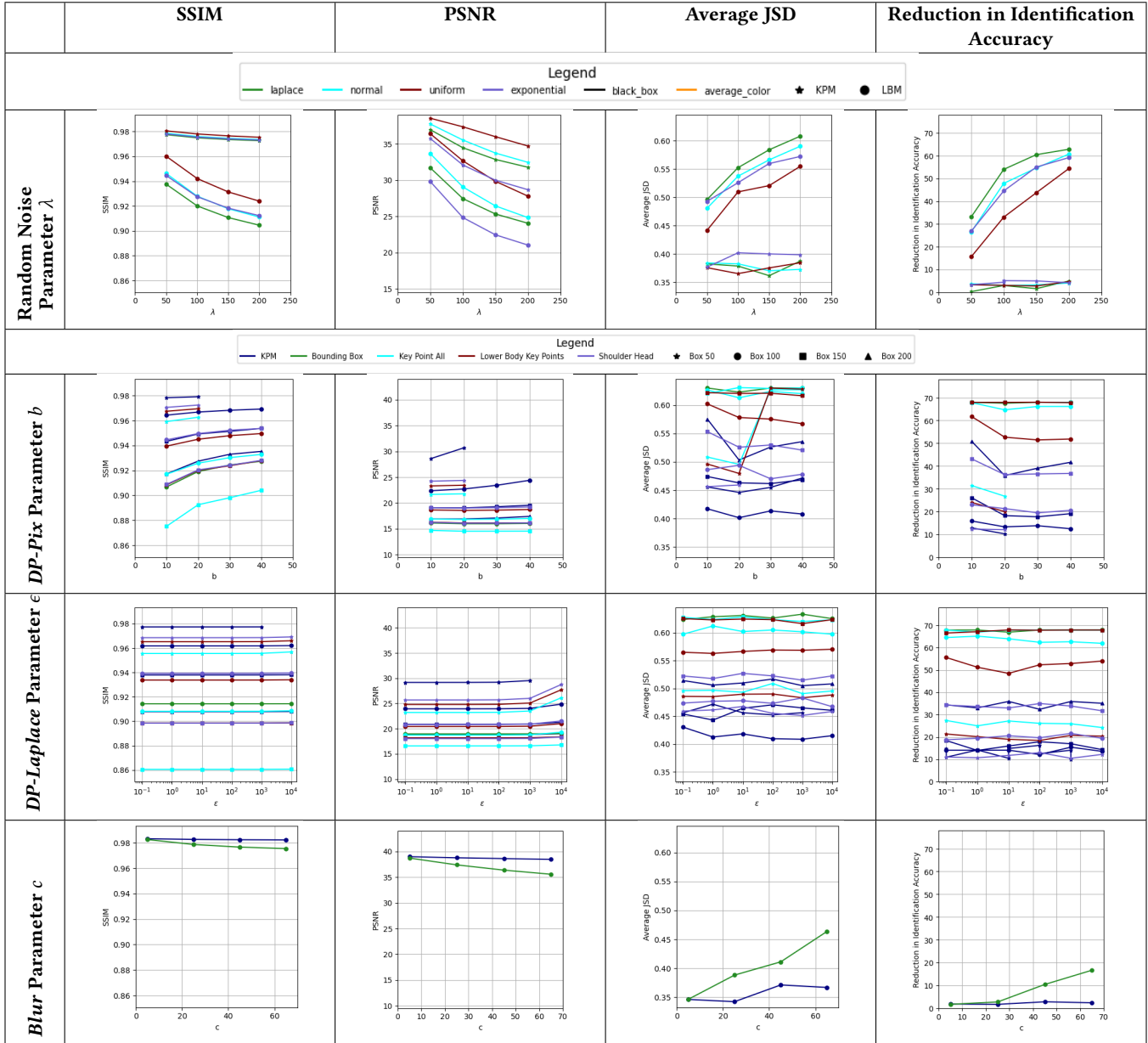


Figure 17: On device implementation of GaitGuard. Raw camera frames are captured from the device's camera. OpenCV is used to detect people in the captured frame. Afterward, noise is applied to the lower half of the detected person, and this noisy frame is released to the network manager.

Evaluation. Application frame rate is a metric that Microsoft uses to qualify the quality of their applications [3]. The suggested application frame rate for the HoloLens 2 is 60 fps to ensure the

Table 4: Inter-Type Parameters vs. SSIM, PSNR, Average, JSD, and Reduction in Identification Accuracy.



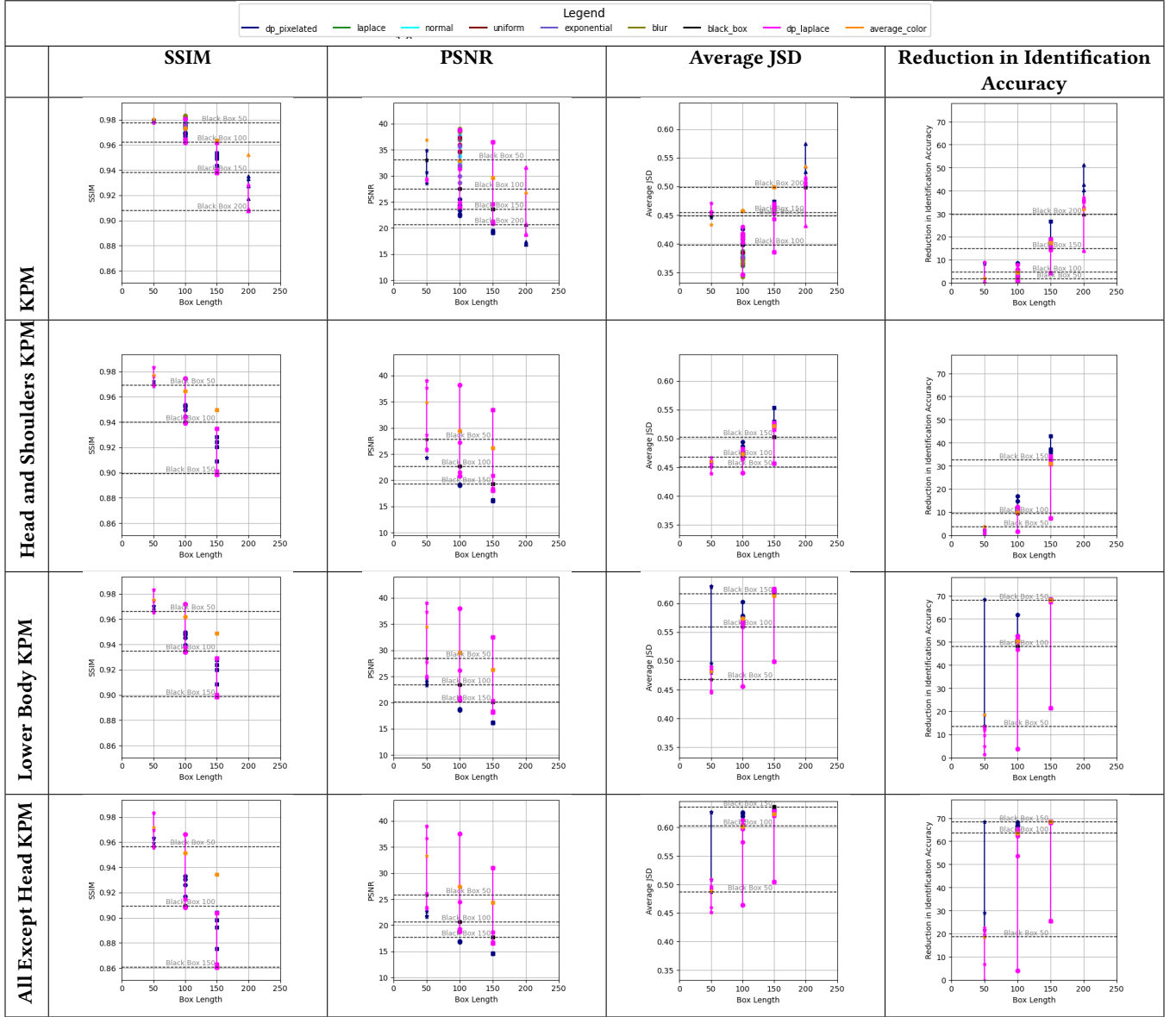
best quality in user experiences [6]. Moreover, it has been reported that the capability of streaming and recording frames from the RGB camera in Hololens 2 containing virtual objects, referred to as Mixed Reality Capture (MRC), has an average frame rate of 30 fps [5].

To assess the ability to deploy **GaitGuard** on Hololens 2, we compare its effect on the recommended frame rate values, which are 60 fps for the application frame rate and 30 fps for the streaming frame rate.

The application frame rate of the on-device implementation of **GaitGuard** is 60 fps. However, to achieve this recommended 60 fps, the rate at which the perturbation was applied to the RGB camera

frame had to be 0.2 fps. This means the on-device implementation of **GaitGuard** could only apply mitigation to one frame every 5 seconds. The application frame rate was unaffected because the **GaitGuard** loop was allocated to run on a background thread, not interfering with the application’s performance. This implementation was motivated by the need for the application fps to be 60 to meet Microsoft’s best performance standard. However, the rate at which **GaitGuard** applies noise is completely unacceptable because multiple steps could have already been completed within these 5 seconds, leaving users vulnerable to attacks. This high latency is because person detection algorithms are computationally intensive

Table 5: Box Lengths Across Different KPM Mitigation vs SSIM, PSNR, Average, JSD, and Reduction in Identification Accuracy.



and do not perform well on a resource-constrained device such as the HoloLens 2.

Insights: The implementation of **GaitGuard** on-device showed impractical due to constrained resources. However, this effectively means that on-device gait leak attacks based on video-based approaches, such as pose estimation or pedestrian detection, are also impractical. Therefore, with the current state of Mixed Reality technology, there is no practical way of gathering gait information using video-based approaches on-device because of the computationally intensive nature of those algorithms.

GaitGuard employs two key functionalities to implement the mitigation. The first involves detecting the lower body keypoints of individuals within the camera frame, while the second entails applying an optimal perturbation configuration. To implement Control

KPM, locating the lower body keypoints in the frame is necessary. Ideally, a pose estimation algorithm like OpenPose would serve this purpose. However, many existing pose estimation libraries have not been adapted for emerging Mixed Reality (MR) technologies, which makes the on-device implementation of Control KPM unfeasible. Additionally, preliminary testing of OpenPose as a mobile server showed that the resulting hardware utility is unacceptable, consistent with literature where real-time mobile implementations of OpenPose generally did not achieve streaming fps above 12 [23]. This highlights that the computational constraint imposed by pose estimation algorithms makes it unsuitable for real-time implementation.

To address this issue, an alternative is the LBM approach, as the mitigation experiments also showed that the LBM approach with DP pixelization had a favorable privacy-utility trade-off, having achieved the same privacy as the baseline with better SSIM. To implement this approach, the lower body area in the frame needs to be identified, indicating that person detection is imperative. Following this, we leverage OpenCV's Histogram of Gradients (HOG) [15] default people detector and HOG's pre-trained SVM classifier.

Initially, **GaitGuard** identifies users in the frame and returns their locations through rectangular bounding boxes. As the bounding box from OpenCV's default people detector covers the entire

body, an ad hoc solution is required to extract the lower body bounds. To approximate the lower body, the height of the obtained rectangular bounds is halved, retaining only the bottom half of the rectangle. Subsequently, **GaitGuard** applies the optimal mitigation to the identified area by generating perturbation of the same size as the lower body bounds across the three image channels (red, green, blue). After this, the perturbed lower body pixels are applied to the camera frame.